Preprint typeset in JHEP style - PAPER VERSION

Cavendish–HEP–07/07

Herwig++ Monte Carlo At Next-To-Leading Order for e^+e^- annihilation and lepton pair production

Oluseyi Latunde-Dada

Cavendish Laboratory, University of Cambridge,
JJ Thomson Avenue, Cambridge CB3 0HE, U.K.
E-mail: seyi@hep.phy.cam.ac.uk

Abstract: This paper describes the MC@NLO method for matching next-to-leading order (NLO) perturbative QCD with the parton shower and hadronization model of the Monte Carlo (MC) event generator Herwig++, for e^+e^- annihilation and Drell-Yan lepton pair production. Details of the event generation method as well as spin, flavour, momentum and colour assignments are presented. We obtain predictions for various distributions which are compared with experimental data.

Keywords: QCD, NLO Computations, Phenomenological Models, Jets, Hadronic colliders.

Contents

1. Introduction

`Herwig++` [1] is a general purpose Monte Carlo event generator used for simulating hard lepton-lepton, lepton-hadron and hadron-hadron collisions. It uses the parton shower approach for initial and final state parton branching processes including colour coherence effects and azimuthal correlations. One example of a process modelled by `Herwig++` is e^+e^- annihilation to $q\bar{q}$ to form two jets (Figure 1). The jet topology (the number of jets) is determined by the hard cross-section of the process whilst the jet structure is determined by `Herwig++` by simulating soft and collinear branching from the primary partons and the conversion of the partonic final states into hadrons (hadronization). Another

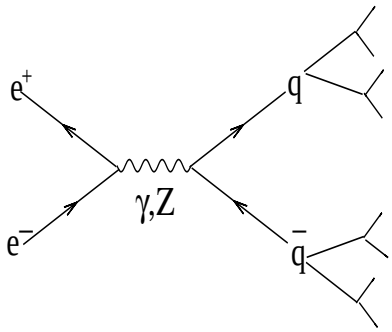

Figure 1: 2 jet formation for e^+e^- annihilation

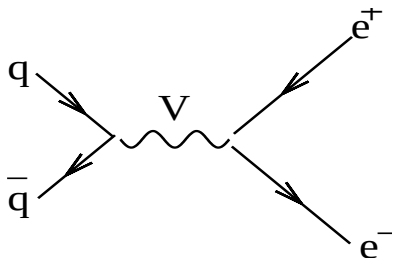

Figure 2: LO diagram for Drell-Yan lepton pair production.

process modelled by `Herwig++` is Drell-Yan lepton pair production from hadron-hadron collisions which is illustrated at leading order in Figure 2. Different methods of matching next-to-leading order calculations to parton shower generators have been proposed and implemented [2, 3, 4, 5, 6, 7]. The aim of this paper is to extend the parton shower simulation to next-to-leading order using the MC@NLO method to include the formation of an extra jet and NLO virtual corrections without any double counting of events. This is illustrated for e^+e^- annihilation in Figure 3. For Drell-Yan lepton pair production, there

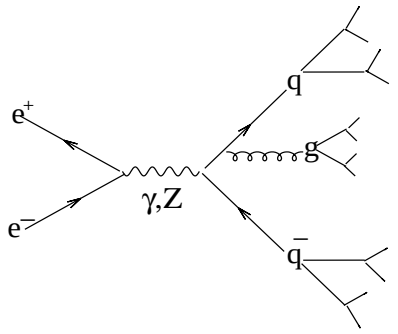

Figure 3: 3 jet formation

are 2 real emission contributions at next-to-leading order. They are the emission of a gluon, $q + \bar{q} \to V + g$ and the QCD Compton subprocess, $q + g \to V + q$. Both are illustrated in Figure 4.

Figure 4: NLO diagrams for lepton pair production.

The generic MC@NLO method is described in [8] and has previously been successfully applied to the hadroproduction of gauge boson pairs [8, 9], heavy quark-antiquark pairs [10] and single-top production [11]. In these applications, the Fortran Monte Carlo event generator `HERWIG` [12] was used to simulate the parton shower and hadronization. In this paper however, the MC@NLO method is applied to the e^+e^- annihilation and Drell-Yan processes using `Herwig++`, a redeveloped version which implements new shower variables and an improved hadronization model [13].

2. e^+e^- annihilation

In the massless limit, the 3-particle cross-section for the process, $e^+e^- \to \gamma^* \to q\bar{q}g$ shown in Figure 5

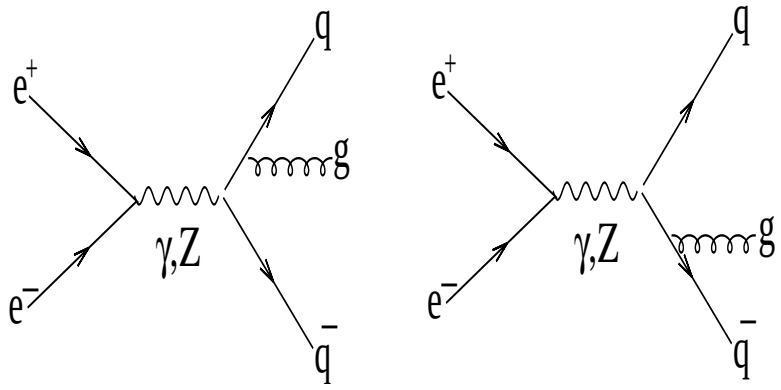

Figure 5: Feynman diagrams for $e^+e^- \to q\bar{q}g$

is given by (neglecting Z boson exchange contributions for the moment)

$$\sigma^{q\bar{q}g} = \sigma_0 \int dx_q dx_{\bar{q}} \frac{\alpha_S}{2\pi} C_F M(x_q, x_{\bar{q}}) \tag{2.1}$$

where

$$\begin{aligned} M(x_q, x_{\bar{q}}) &= \frac{x_q^2 + x_{\bar{q}}^2}{(1-x_q)(1-x_{\bar{q}})}\,, \\ x_q &= \frac{2E_q}{\sqrt{s}}\,, \\ x_{\bar{q}} &= \frac{2E_{\bar{q}}}{\sqrt{s}}\,, \\ \sigma_0 &= 3\sum_q {Q_q}^2 \frac{4\pi\alpha^2}{3s}\,, \end{aligned} \tag{2.2}$$

$C_F = 4/3$ (for the case of SU(3)colour representations), and the integration region is: $0 \le x_q, x_{\bar{q}} \le 1, x_q + x_{\bar{q}} \ge 1$ [14].

The integrand in (2.1) is divergent at $x_q, x_{\bar{q}} = 1$ where the gluon is collinear with the quark or antiquark or where the gluon is soft. As we shall see shortly, these singularities are cancelled out in the total cross-section to next-to-leading order in α_S. Using dimensional regularization, (2.1) can be evaluated to give,

$$\sigma^{q\bar{q}g}(\epsilon) = \sigma_0 \frac{C_F \alpha_S}{2\pi} H(\epsilon) \left[\frac{2}{\epsilon^2} + \frac{3}{\epsilon} + \frac{19}{2} - \pi^2 + O(\epsilon) \right] \tag{2.3}$$

where

$$\begin{aligned} \epsilon &= \frac{1}{2}(4-n)\,, \\ H(\epsilon) &= \frac{3(1-\epsilon)}{(3-2\epsilon)\Gamma(2-2\epsilon)} (4\pi)^{2\epsilon}\,, \\ &= 1 + O(\epsilon) \end{aligned} \tag{2.4}$$

and n = number of dimensions.

The total cross-section to order α_S is obtained by adding the contributions from the leading order and virtual gluon Feynman diagrams in Figure 6 to (2.3). This contribution

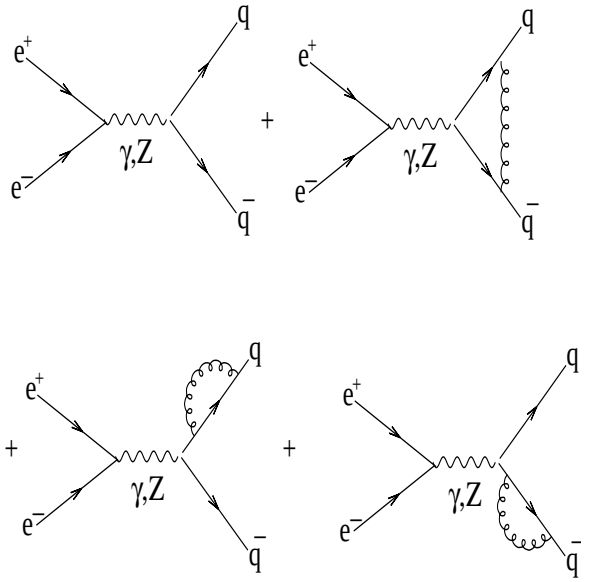

Figure 6: Leading order and virtual gluon Feynman diagrams

is

$$\sigma_0 \left[1 + \frac{C_F \alpha_S}{2\pi} H(\epsilon) \left\{ -\frac{2}{\epsilon^2} - \frac{3}{\epsilon} - 8 + \pi^2 + O(\epsilon) \right\} \right] . \tag{2.5}$$

Taking $C_F = 4/3$ (for the SU(3) colour group), the total cross-section is found to be [14],

$$\sigma_{\text{total}} = \sigma_0 \left[1 + \frac{\alpha_S}{\pi} + O({\alpha_S}^2) \right] . \tag{2.6}$$

For massless partons, the QCD correction at O(α_S) is independent of the nature of the exchanged boson. Hence at this order for Z boson exchange,

$$\sigma_{\text{total}} = \sigma_0^Z [1 + \frac{\alpha_S}{\pi}] \tag{2.7}$$

where

$$\sigma_0^Z = 3\sum_q ({A_q}^2 + {V_q}^2)({A_e}^2 + {V_e}^2)\frac{4\pi\alpha^2\kappa^2}{3\Gamma^2}\,,$$
$$\kappa = \frac{\sqrt{2}G_F M_z^2}{16\pi\alpha}\,, \tag{2.8}$$

A_q, V_q, A_e and V_e are the axial and vector coupling constants for the quarks and leptons respectively, G_F is the Fermi constant, M_Z is the pole mass of the Z boson and Γ is the total decay width of the Z boson. Note that this is the cross-section at $\sqrt{s} = M_Z$.

As was mentioned earlier, it can be seen that the collinear and soft singularities in (2.3) have been cancelled in σ_{total}. However, writing σ_{total} as a sum of two separate parts (2.3) and (2.5), makes it possible to generate a Monte-Carlo events in $x_q, x_{\bar{q}}$ space which can be fed into `Herwig++` to simulate 2 and 3-jet processes. This is the subject of section 3.

3. MC@NLO method

Writing σ_{total} explicitly as the sum of equations (2.3) and (2.5) gives

$$\sigma_{\text{total}} = \sigma_0\left[1 + \frac{C_F\alpha_S}{2\pi}H(\epsilon)\left(-\frac{2}{\epsilon^2} - \frac{3}{\epsilon} - 8 + \pi^2 + O(\epsilon)\right)\right.$$
$$\left. +\ \frac{C_F\alpha_S}{2\pi}H(\epsilon)\left(\frac{2}{\epsilon^2} + \frac{3}{\epsilon} + \frac{19}{2} - \pi^2 + O(\epsilon)\right)\right] \tag{3.1}$$

This can be re-written in integral form as

$$\sigma_{\text{total}} = \sigma_0\int dx_q dx_{\bar{q}}\left[2 - \frac{\alpha_S}{2\pi}C_F\left\{M(x_q, x_{\bar{q}}, \epsilon) - 3\right\} + \frac{\alpha_S}{2\pi}C_F M(x_q, x_{\bar{q}}, \epsilon)\right] \tag{3.2}$$

where

$$M(x_q, x_{\bar{q}}, \epsilon) = \frac{H(\epsilon)}{[(1-x_q)(1-x_{\bar{q}})(1-x_g)]^\epsilon}\left[\frac{(1-\epsilon)(x_q^2 + x_{\bar{q}}^2) + 2\epsilon(1-x_g)}{(1-x_q)(1-x_{\bar{q}})} - 2\epsilon\right] \tag{3.3}$$

is the $e^+e^- \to q\bar{q}g$ hard matrix element and $x_g = 2 - x_q - x_{\bar{q}}$. Now, if we define a functional F_i as the functional which represents hadronic final states generated by the parton shower starting from a configuration i, a generating functional for the process $e^+e^- \to$ hadrons can be written as

$$F = \sigma_0\int dx_q dx_{\bar{q}}\left[F_{q\bar{q}}\left\{2 - \frac{\alpha_S}{2\pi}C_F\left(M(x_q, x_{\bar{q}}) - 3\right)\right\} + F_{q\bar{q}g}\frac{\alpha_S}{2\pi}C_F M(x_q, x_{\bar{q}})\right] \tag{3.4}$$

where $F_{q\bar{q}}$ is the functional representing the shower final states resulting from the process $e^+e^- \to q\bar{q}$ and $F_{q\bar{q}g}$ represents the final states from $e^+e^- \to q\bar{q}g$. We have set $\epsilon = 0$ so that $H(\epsilon) = 1$ and $M(x_q, x_{\bar{q}}, \epsilon) = M(x_q, x_{\bar{q}})$ which is defined in (2.1).

This would be wrong however because configurations starting with $q\bar{q}$, would also radiate quasi-collinear gluons, with a distribution, $M_C(x_q, x_{\bar{q}})$ given by the parton shower.

Likewise, configurations with $q\bar{q}g$ would generate $q\bar{q}$-like configurations if the gluon is quasi-collinear to the quark or antiquark. $M_C(x_q, x_{\bar{q}})$ is the parton shower branching cross-section, which in the massless case is given in `Herwig++` by

$$\frac{\alpha_S}{2\pi} C_F M_C(x_q, x_{\bar{q}}) = \frac{\alpha_S}{2\pi} C_F \frac{1 + \left(\frac{x_q + x_{\bar{q}} - 1}{x_q}\right)^2}{(1 - x_{\bar{q}})(1 - x_q)} \tag{3.5}$$

for a gluon branching quasi-collinearly off the antiquark. (Interchange x_q and $x_{\bar{q}}$ for a gluon branching off the quark). This can be derived from the quasi-collinear splitting function defined terms of the `Herwig++` evolution variables, z and $\tilde{q}$ in (3.6) [15]:

$$dP(q \to qg) = \frac{C_F}{2\pi} \alpha_S [z^2 (1 - z)^2 \tilde{q}^2] \frac{d\tilde{q}^2}{\tilde{q}^2} \frac{dz}{1 - z} [1 + z^2 - \frac{2m^2}{z\tilde{q}^2}] \tag{3.6}$$

where z is the momentum fraction of the quark after gluon emission relative to the parent quark and $\tilde{q}$ is an angular variable related to the relative transverse momentum, $\mathbf{p_T}$ of the quark after gluon emission via:

$$| \mathbf{p_T} | = \sqrt{(1 - z)^2)(z^2 \tilde{q}^2 - \mu^2) - z {Q_g}^2}\,, \tag{3.7}$$

$\mu = \max(m, Q_g)$ and ${Q_g}^2$ is the minimum virtuality for the quarks and gluons which is required to define a resolvable emission. The Dalitz plot variables x_q and $x_{\bar{q}}$ are related to the evolution variables z and $\tilde{q}$ via;

$$\begin{aligned} x_q &= 1 - z(1 - z)\kappa\,, \\ x_{\bar{q}} &= (2 - x_q) r + (z - r)\sqrt{x_q^2 - 4\rho} \end{aligned} \tag{3.8}$$

where

$$\begin{aligned} \rho &= \frac{m^2}{s}\,, \\ r &= \frac{1}{2}\left(1 + \frac{\rho}{1 + \rho - x_q}\right)\,, \\ z &= r + \frac{x_{\bar{q}} - (2 - x_q) r}{\sqrt{x_q^2 - 4\rho}}\,, \\ \kappa &= \frac{\tilde{q}^2}{s}\,. \end{aligned} \tag{3.9}$$

By changing the evolution variables in (3.6) to the Dalitz plot variables in the limit where $m = \rho = 0$, (3.5) can be derived. The Jacobian factor for the transformation is

$$z(1 - z)\sqrt{x_q^2 - 4\rho}\,. \tag{3.10}$$

The equations given above apply to a radiating antiquark. For a radiating quark, interchange x_q and $x_{\bar{q}}$. Imposing the condition

$$\kappa < \frac{1}{2}(1 + \sqrt{1 - 4\rho}) \tag{3.11}$$

defines the regions of the phase space covered by the parton showers i.e the quark and antiquark jets. In the massless limit this yields the function Θ_{PS} in (3.12) which defines the phase space regions J_q, $J_{\bar{q}}$ and D in Figure 7.

$$\Theta_{PS} = \Theta[(1-x_q)(x_q+x_{\bar{q}}-1)-x_{\bar{q}}^2(1-x_{\bar{q}})]+\Theta[(1-x_{\bar{q}})(x_q+x_{\bar{q}}-1)-x_q^2(1-x_q)]\ . \quad (3.12)$$

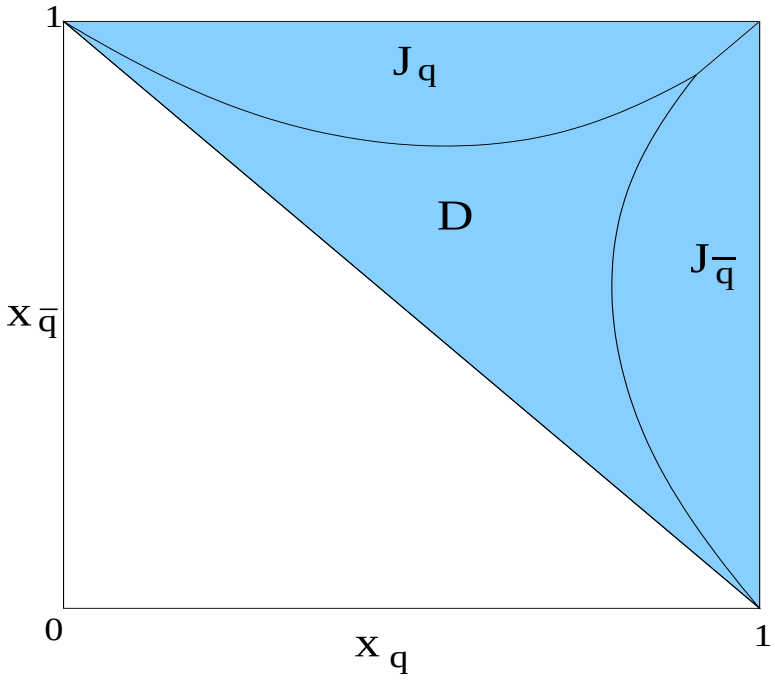

Figure 7: Phase space for $x_q, x_{\bar{q}}$ showing hard (D) and soft/collinear ($J_q, J_{\bar{q}}$) gluon emission regions.

The full integration region is shown shaded in the figure above. Regions J_q and $J_{\bar{q}}$ include soft and quasi-collinear gluon emission events whilst region D includes hard and non-collinear gluon emission events, giving rise to additional jets.

Having defined M_C, we can now obtain the correct overall functional by subtracting the integral of (3.5) from the second term in (3.4) and adding it to the first term:

$$F = \sigma_0 \int dx_q dx_{\bar{q}} \left[F_{q\bar{q}} \left\{ 2 - \frac{\alpha_S}{2\pi} C_F \left(M - M_C - 3 \right) \right\} + F_{q\bar{q}g} \frac{\alpha_S}{2\pi} C_F (M - M_C) \right] \ . \quad (3.13)$$

This subtraction is relevant only to regions J_q and $J_{\bar{q}}$ in Figure 7 which include soft and collinear emission events. In region D, which contains hard emission events, we simply integrate the hard matrix element, $M(x_q, x_{\bar{q}})$ over the region. Therefore the overall generating functional can be written as

$$\begin{aligned} F = \sigma_0 \Bigg[& \int_J dx_q dx_{\bar{q}} \left[F_{q\bar{q}} \left\{ 2 - \frac{\alpha_S}{2\pi} C_F (M - M_C - 3) \right\} + F_{q\bar{q}g} \frac{\alpha_S}{2\pi} C_F (M - M_C) \right] \\ & + \int_D dx_q dx_{\bar{q}} \left[F_{q\bar{q}} \left\{ 2 - \frac{\alpha_S}{2\pi} C_F (M - 3) \right\} + F_{q\bar{q}g} \frac{\alpha_S}{2\pi} C_F M \right] \Bigg] \end{aligned} \quad (3.14)$$

where J denotes the region $J_q \cup J_{\bar{q}}$. Note that the total cross-section can be retrieved by making the substitution $F_{q\bar{q}}, F_{q\bar{q}g} = 1$ in (3.14) as shown.

$$\sigma_{\text{total}} = \sigma_0 \left[\int_J dx_q dx_{\bar{q}} \left\{ 2 - \frac{\alpha_S}{2\pi} C_F (M - M_C - 3) + \frac{\alpha_S}{2\pi} C_F (M - M_C) \right\} + \int_D dx_q dx_{\bar{q}} \left\{ 2 - \frac{\alpha_S}{2\pi} C_F (M - 3) + \frac{\alpha_S}{2\pi} C_F M \right\} \right] . \tag{3.15}$$

The 'Hit or Miss' Monte Carlo method was used to evaluate the integrals and the events were generated using the importance sampling method. The algorithm is described in Appendix A.

4. Heavy quarks

So far, we have discussed the limit in which the quark and anti-quark are massless. We shall now discuss the case where heavy flavour quarks are produced i.e. charm quarks of mass 1.6 GeV and bottom quarks of mass 5 GeV. There are two ways in which this can be treated. Both methods are described below.

4.1 Method 1: Using the heavy quark matrix element

The 3-particle differential cross-section for the process $e^+e^- \to V \to Q\bar{Q}g$, where V represents a vector current like the photon is given by [16];

$$\frac{1}{\sigma_V} \frac{d^2\sigma_V}{dx_Q dx_{\bar{Q}}} = \frac{\alpha_S}{2\pi} \frac{C_F}{v} \left[\frac{(x_Q^2 + 2\rho)^2 + (x_{\bar{Q}}^2 + 2\rho)^2 + \zeta_V}{(1 + 2\rho)(1 - x_Q)(1 - x_{\bar{Q}})} - \frac{2\rho}{(1 - x_Q)^2} - \frac{2\rho}{(1 - x_{\bar{Q}})^2} \right] \tag{4.1}$$

where

$$\begin{aligned} \rho &= \frac{m_Q^2}{s} , \\ v &= \sqrt{1 - 4\rho} , \\ \zeta_V &= -8\rho(1 + 2\rho) , \\ \sigma_V &= \sigma_0 (1 + 2\rho) v . \end{aligned} \tag{4.2}$$

For an axial current contribution $e^+e^- \to A \to Q\bar{Q}g$, we have

$$\frac{1}{\sigma_A} \frac{d^2\sigma_A}{dx_Q dx_{\bar{Q}}} = \frac{\alpha_S}{2\pi} \frac{C_F}{v} \left[\frac{(x_Q^2 + 2\rho)^2 + (x_{\bar{Q}}^2 + 2\rho)^2 + \zeta_A}{v^2 (1 - x_Q)(1 - x_{\bar{Q}})} - \frac{2\rho}{(1 - x_Q)^2} - \frac{2\rho}{(1 - x_{\bar{Q}})^2} \right] \tag{4.3}$$

where

$$\begin{aligned} \zeta_A &= 2\rho[(3 + x_g)^2 - 19 + 4\rho] , \\ \sigma_A &= \sigma_0 v^3 . \end{aligned} \tag{4.4}$$

σ_V and σ_A are the Born cross-sections for heavy quark production by a vector and axial current respectively whilst σ_0 is the massless quark Born cross-section.

Since the partons are massive, the phase space available for gluon emission is reduced. It is determined by the triangle relation:

$$\Delta(x_Q^2 - \rho, x_{\bar{Q}}^2 - \rho, x_g^2) \leq 0 \tag{4.5}$$

where $\Delta(a,b,c) = a^2+b^2+c^2-2ab-2ac-2bc$. This is equivalent to satisfying the condition

$$(1-x_Q)(1-x_{\bar{Q}})(x_Q + x_{\bar{Q}} - 1) > \rho(2 - x_Q - x_{\bar{Q}})^2 \tag{4.6}$$

in the phase space.

Just as in the massless limit, the phase space region can again be split into 2 regions J_Q and $J_{\bar{Q}}$, containing soft and quasi-collinear gluon emission events and a region D containing hard and non-collinear emission events as shown in Figure 8. There is also an additional region labeled O outside the phase space which as we shall see in (4.9) generates 2-jet events.

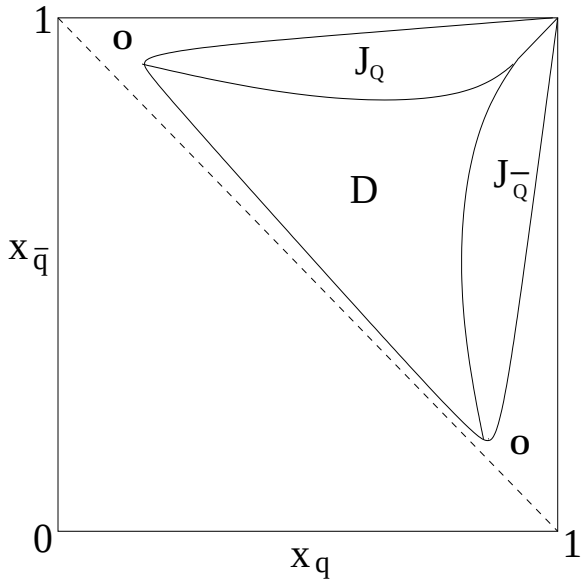

Figure 8: Heavy flavour phase space for $x_Q, x_{\bar{Q}}$ showing hard (D) and soft ($J_Q, J_{\bar{Q}}$) gluon emission regions. Not to scale

As in the massless case, the total 3-particle cross-section to $O(\alpha_S)$ is calculated by adding leading order and virtual gluon contributions to the integrals of (4.1) and (4.3) over the phase space in Figure 8. This yields for photon exchange [14]

$$\sigma_{\text{total}} = \sigma_V \left[1 + c_1 \frac{\alpha_S}{\pi}\right] \tag{4.7}$$

where $c_1 \approx 1 + 12\rho$ [17].

For Z boson exchange, to $O(\alpha_S)$, the cross-section is given by [14]

$$\sigma_{\text{total}} = \sigma_V \left[1 + c_1 \frac{\alpha_S}{\pi}\right] + \sigma_A \left[1 + d_1 \frac{\alpha_S}{\pi}\right] \tag{4.8}$$

where $d_1 \approx 1 - 22\rho$ [17].

Following the same procedure as for the massless case, Monte Carlo events can be generated by writing σ_{total} explicitly. For example, the jet generating functional, F can now be written as;

$$\begin{aligned} F = \sigma_V \Bigg[& \int_O dx_{\bar{Q}} dx_Q F_{Q\bar{Q}} \left\{ 2 + 3c_1 \frac{\alpha_S}{2\pi} C_F \right\} \\ & + \int_D dx_Q dx_{\bar{Q}} \left[F_{Q\bar{Q}} \left\{ 2 - \frac{\alpha_S}{2\pi} C_F (M - 3c_1) \right\} + F_{Q\bar{Q}g} \frac{\alpha_S}{2\pi} C_F M \right] \\ & + \int_J dx_Q dx_{\bar{Q}} \left[F_{Q\bar{Q}} \left\{ 2 - \frac{\alpha_S}{2\pi} C_F (M - M_C - 3c_1) \right\} + F_{Q\bar{Q}g} \frac{\alpha_S}{2\pi} C_F (M - M_C) \right] \Bigg] \end{aligned} \quad (4.9)$$

where $J = J_Q \cup J_{\bar{Q}}$, M is the differential cross-section defined in (4.1) and M_C is the heavy quark quasi-collinear branching probability given in (3.6).
Just as in the massless limit, setting $F_{Q\bar{Q}}, F_{Q\bar{Q}g} = 1$ in (4.9) recovers the vector exchange part of σ_{total} in (4.8). The only difference is the integral over the region O outside the phase space which is required to recover the full cross-section. As before, the coefficients of $F_{Q\bar{Q}}$ and $F_{Q\bar{Q}g}$ generate 2-jet and 3-jet events respectively. Details of the evaluation of the integrals can be found in Appendix C. Event generation follows the same lines as described on Appendix A.

4.2 Method 2: Using the massless quark matrix element

Since the masses of the charm and bottom quarks (1.6 and 5 GeV respectively) are small compared to the center of mass energy at the Large Electron-Positron (LEP) collider (91.2 GeV), they can in the first approximation be assumed to be massless. Hence, the massless matrix element can be used to obtain the 4-momentum distributions for charm and bottom quarks as described above for up, down and strange quarks. This is less rigorous than the method described in section 4.1 but it has the advantage of a smoother distribution of events due to the unweighting procedure being more efficient. This is the method used in this paper.

5. Results on e^+e^- annihilation

The methods described above were used to generate e^+e^- events for comparison with LEP 1 data. Details of the assignment of partonic final-state properties are described in Appendix D. Figures 9-13 show comparisons of event shape distributions obtained from our results and LEP 1 data. The massless quark matrix element method described in section 4.2 was used for heavy quark generation. Also compared are event shapes obtained from `Herwig++` with the matrix element correction switched on. This is the method whereby emissions are only accepted into the dead region D of the phase space at a rate given by the matrix element. In both cases `Herwig++` version 2.0.1 was used. The hadronization scale which is the scale at which the shower is turned off was set to the default value of 0.631 GeV and the 2-loop α_S value was used.

Figures 14-16 show comparisons of identified particle spectra from events of different flavour with SLD data [18]. In general we are able to give a good description of the data with the MC@NLO method. The MC@NLO results for the LEP event shape distributions do not differ greatly from the matrix element correction results. For example, the thrust distribution appears to suffer from the same problem of generating too much transverse structure, leading to less two-jet like event shapes.

However, despite the similarity in results, we can be confident that the MC@NLO results are normalised to the full NLO cross-section including virtual corrections unlike the matrix element correction.

The identified particle spectra includes hadron momenta distributions from heavy quark production. Although the results are similar, in some cases the MC@NLO results are slightly better than the matrix element correction results. This can be attributed to the better treatment of the heavy quark production cross-sections in the relevant plots.

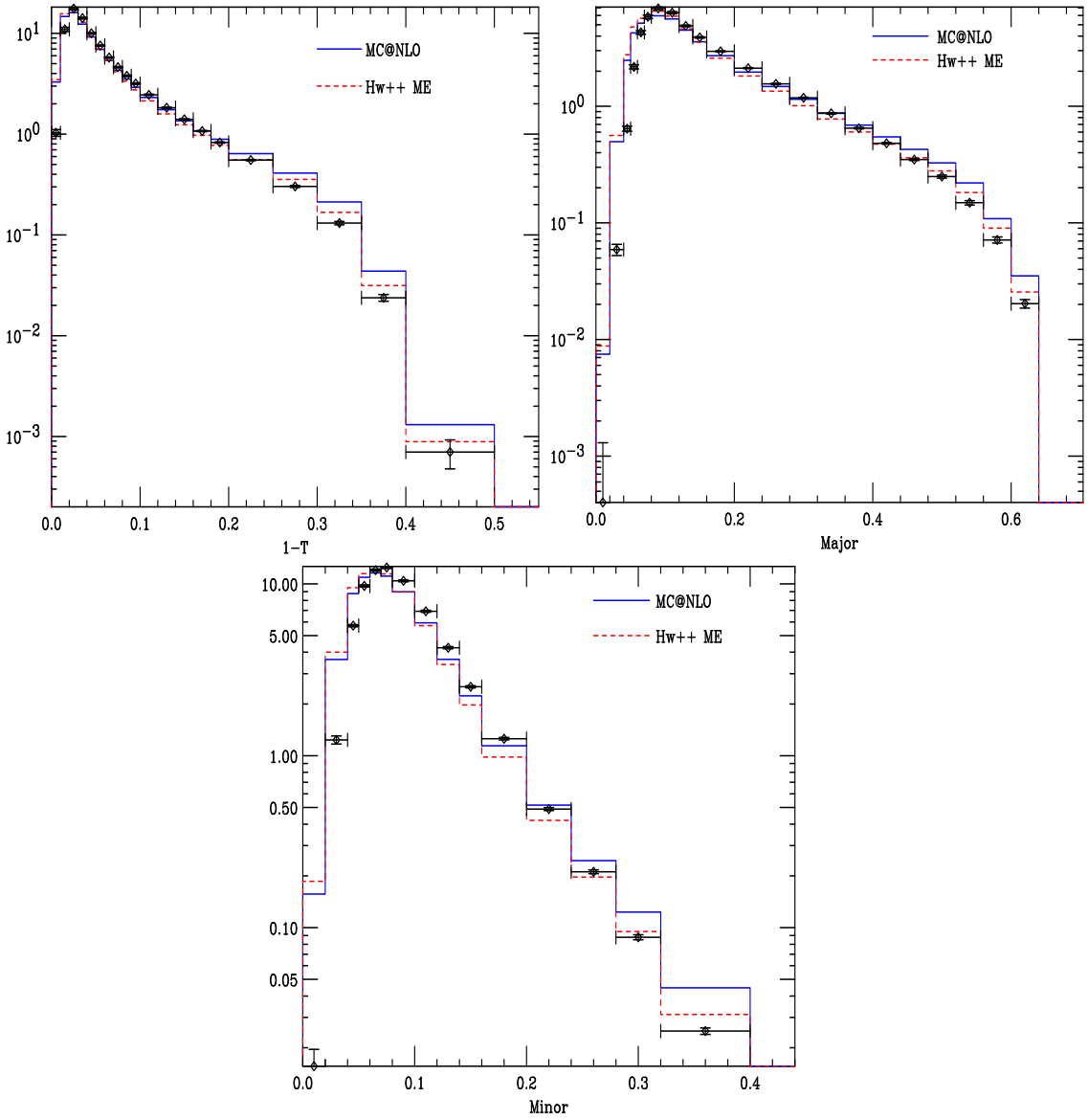

Figure 9: Thrust, Thrust major and Thrust minor. Data from [19].

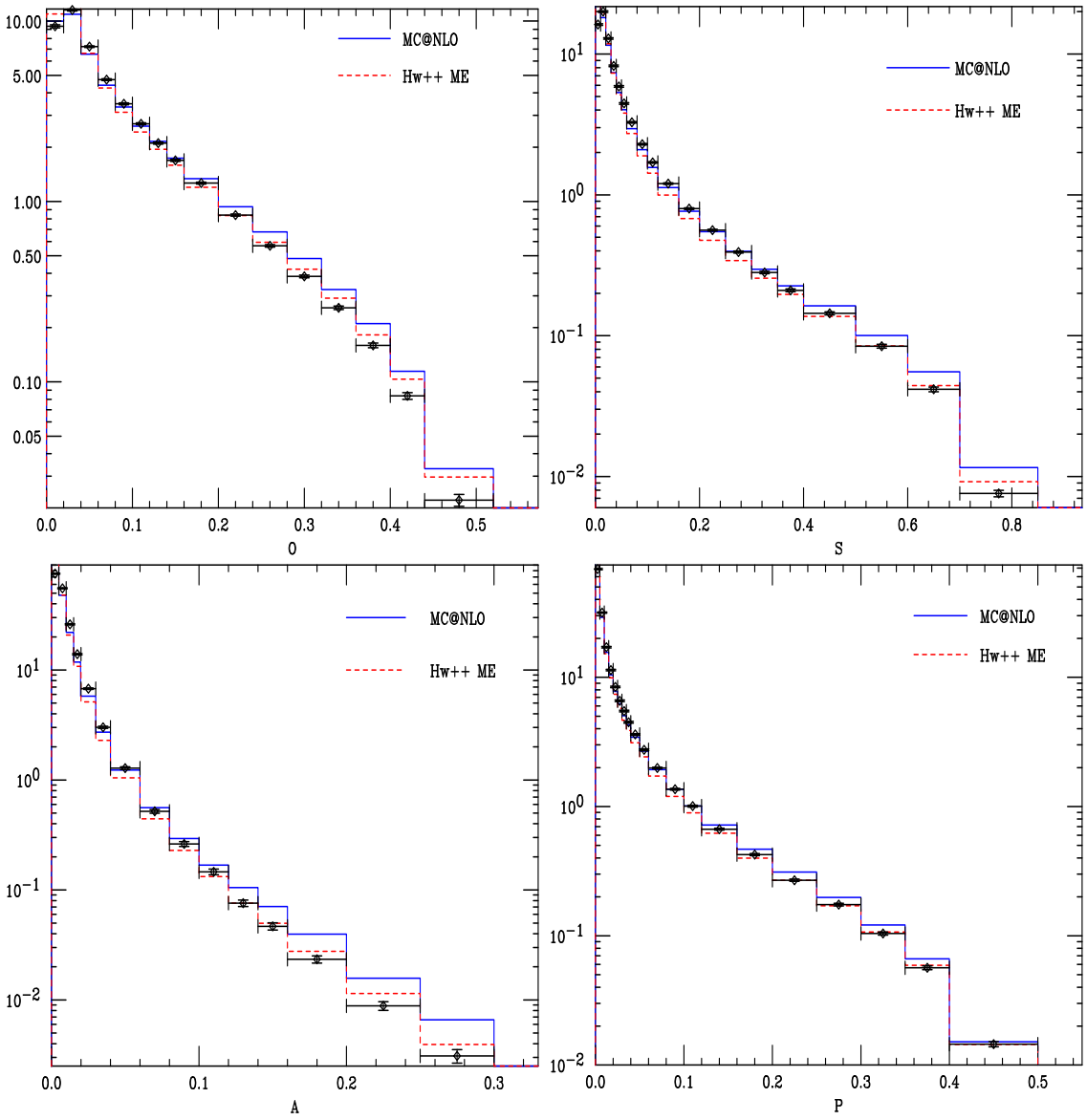

Figure 10: Oblateness, Sphericity, Aplanarity and Planarity distributions. Data from [19].

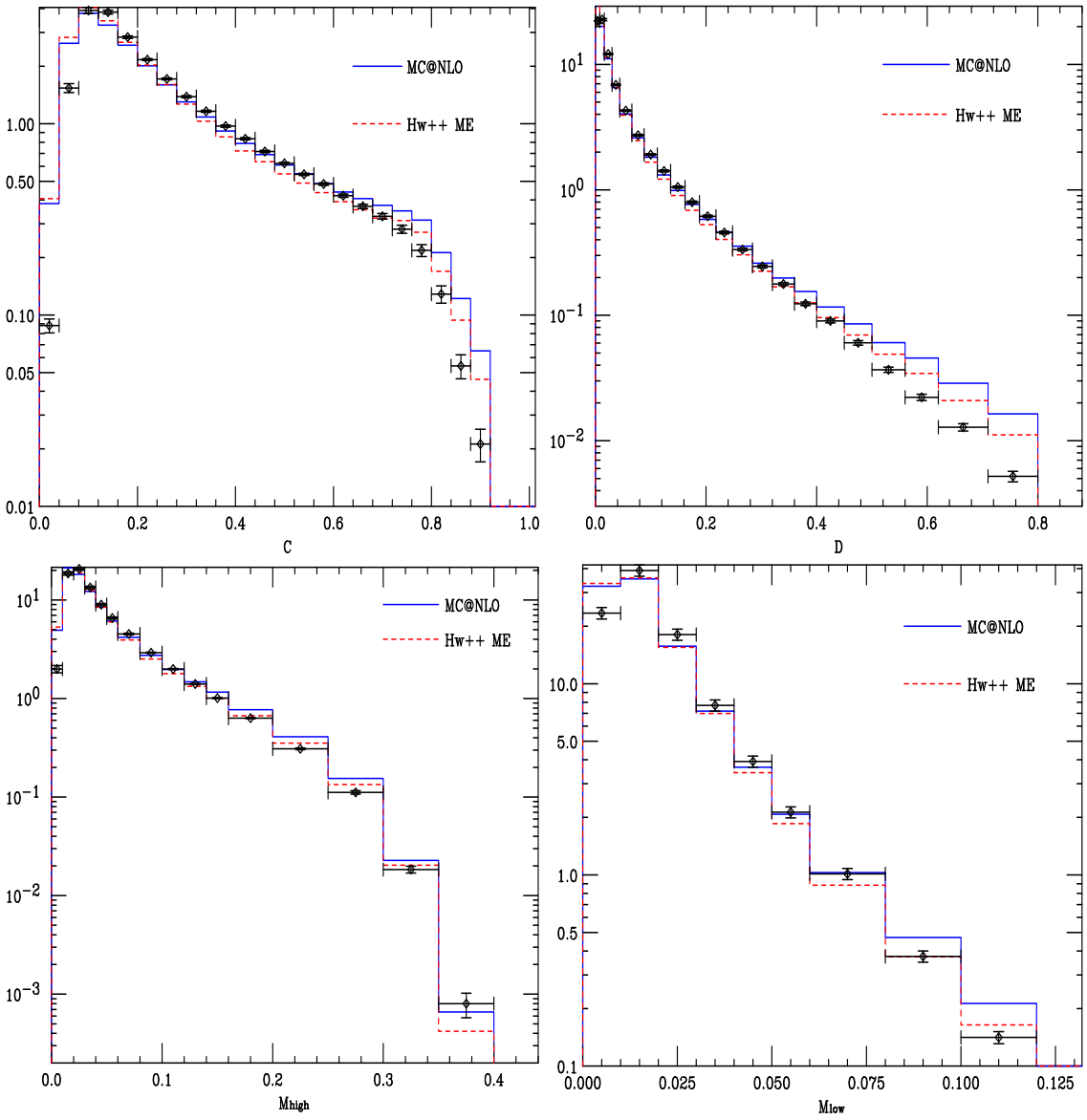

Figure 11: C Parameter and D Parameter distributions and the high, M_{high} and low, M_{low} hemisphere masses. Data from [19].

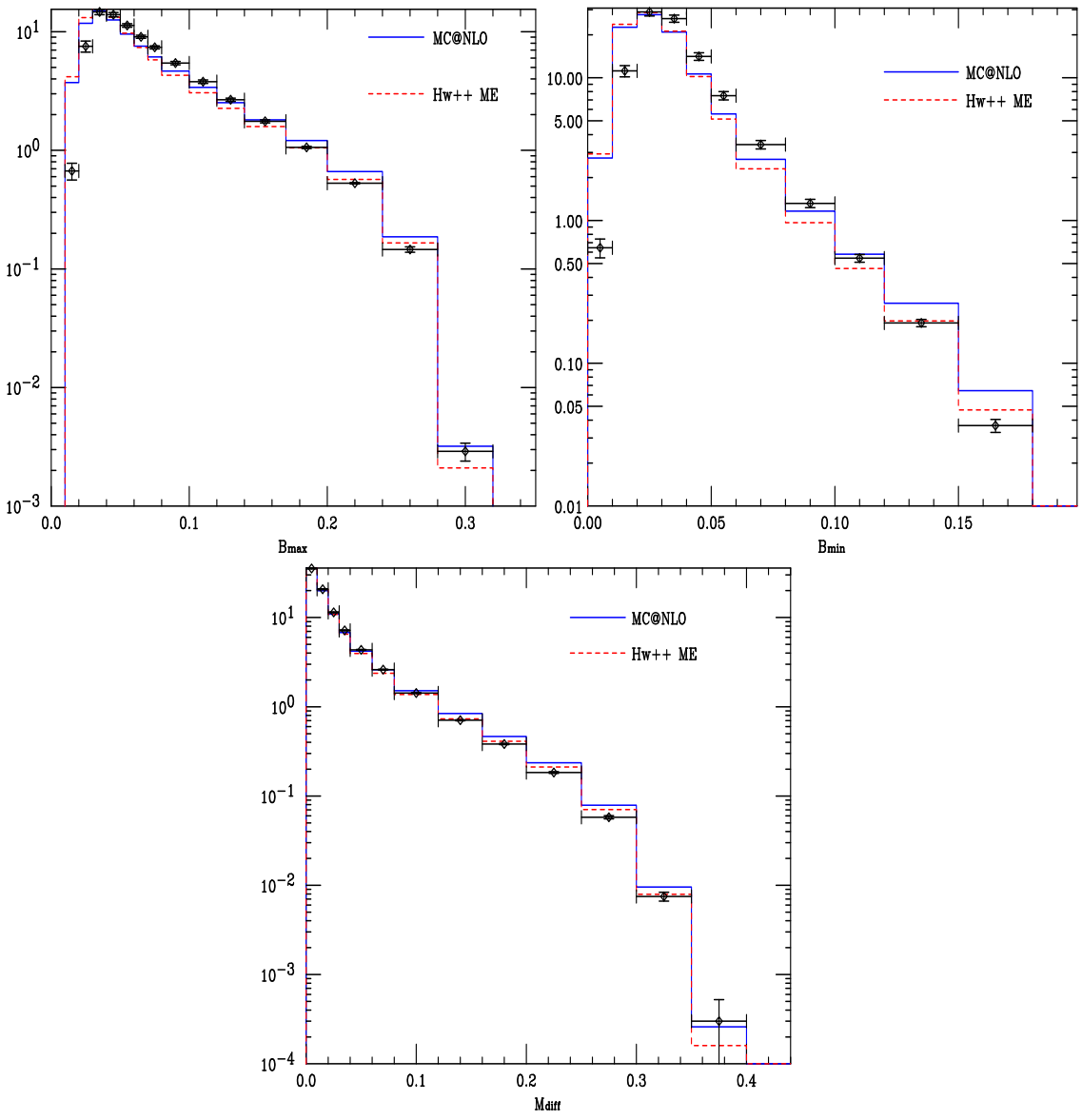

Figure 12: The wide and narrow jet broadening measures $B_{\max}$ and $B_{\min}$ and the difference in hemisphere masses, M_{diff}. Data from [19].

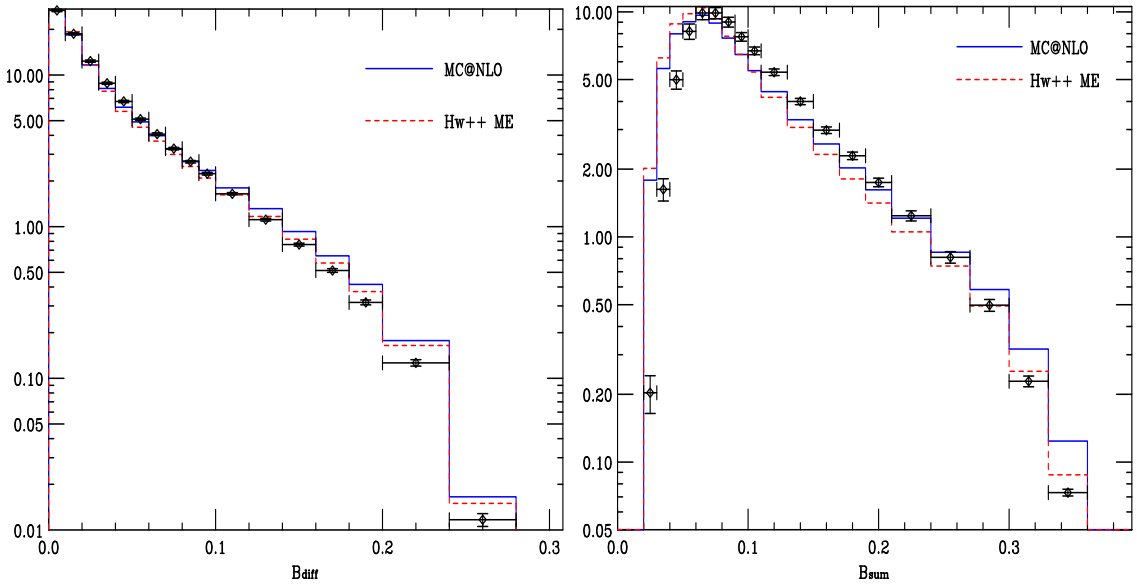

Figure 13: The difference and sum of jet broadenings B_{diff} and B_{sum}. Data from [19].

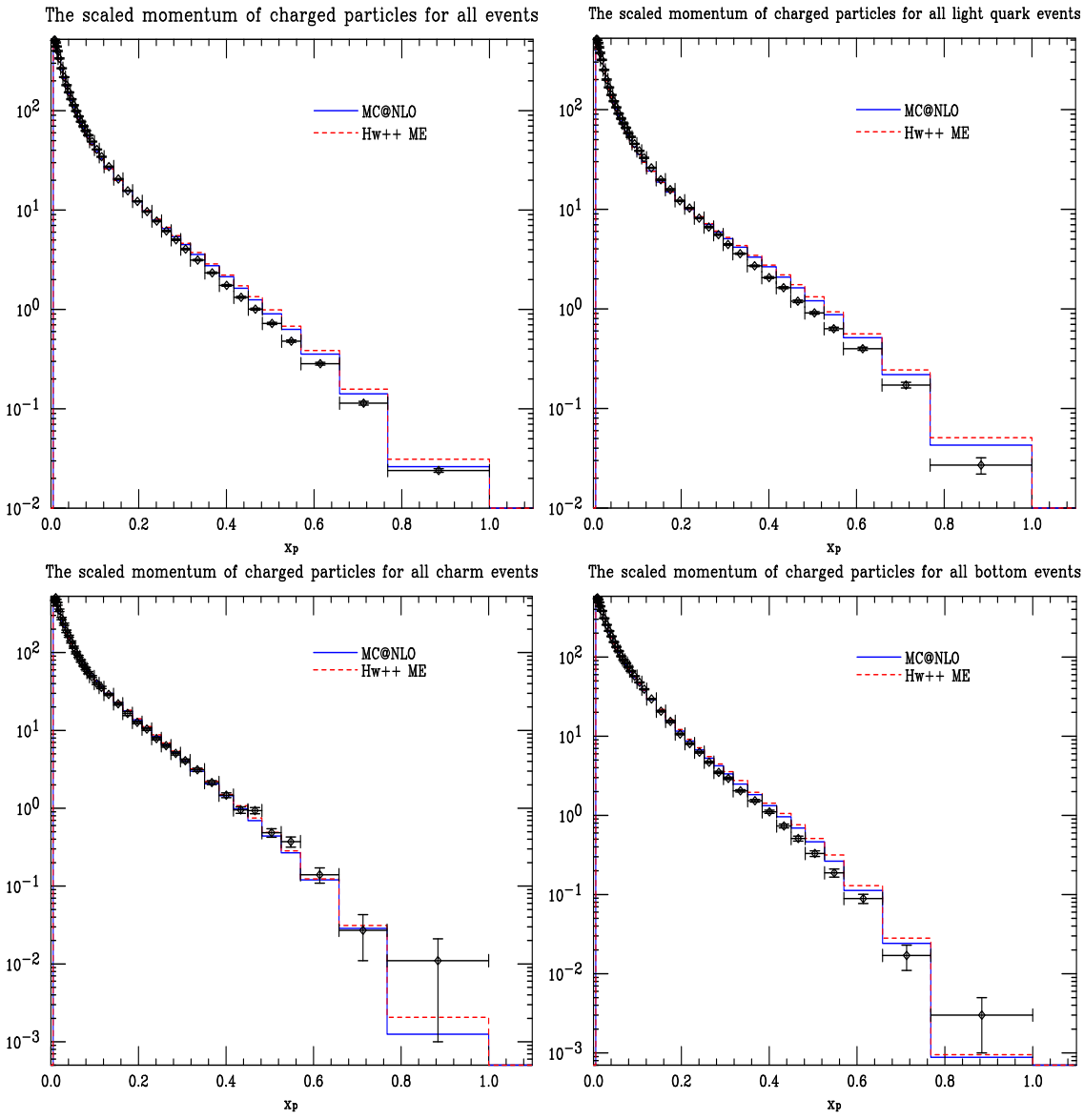

Figure 14: The scaled momentum distributions of all charged particles.

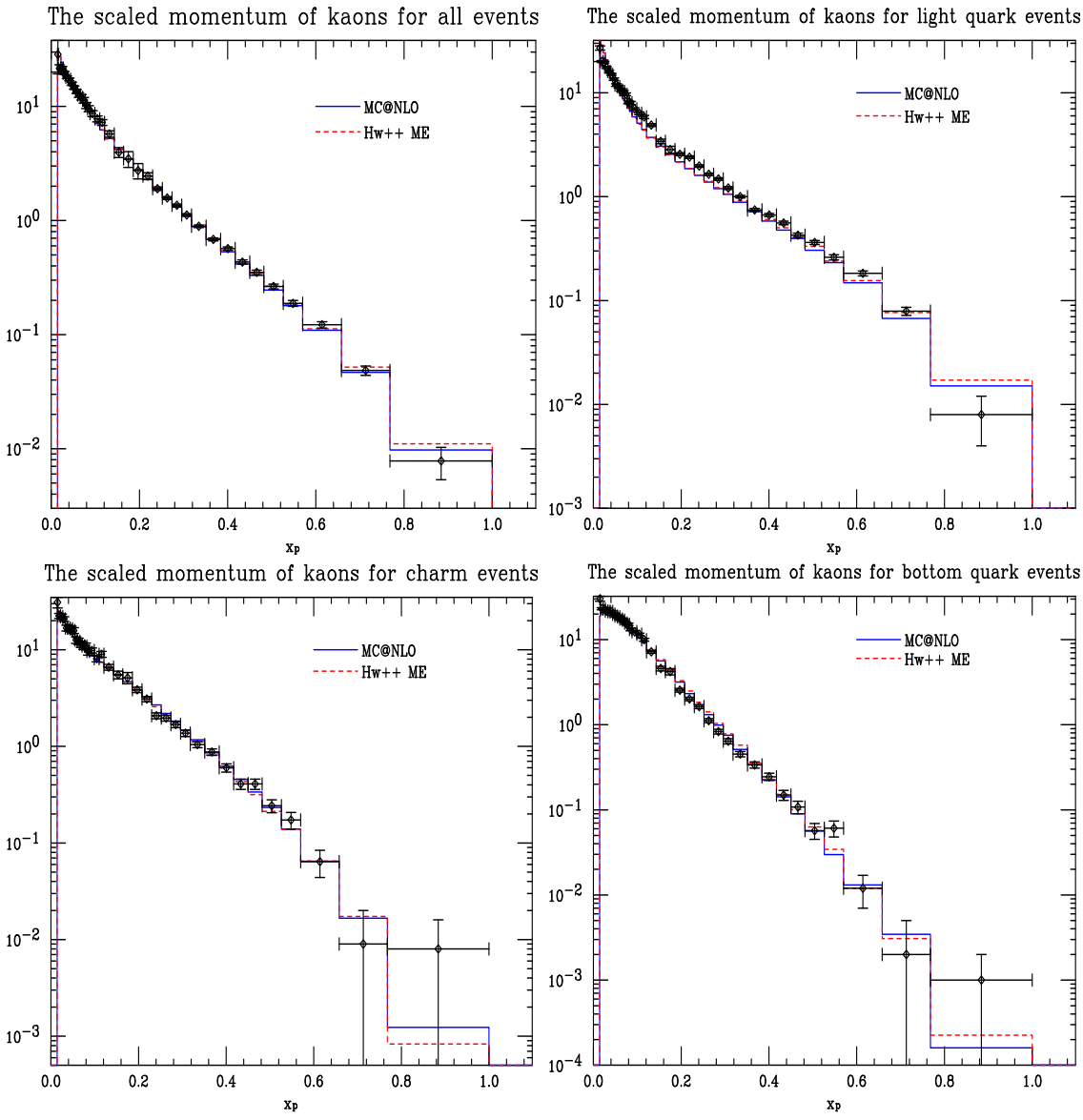

Figure 15: The scaled momentum distributions of kaons.

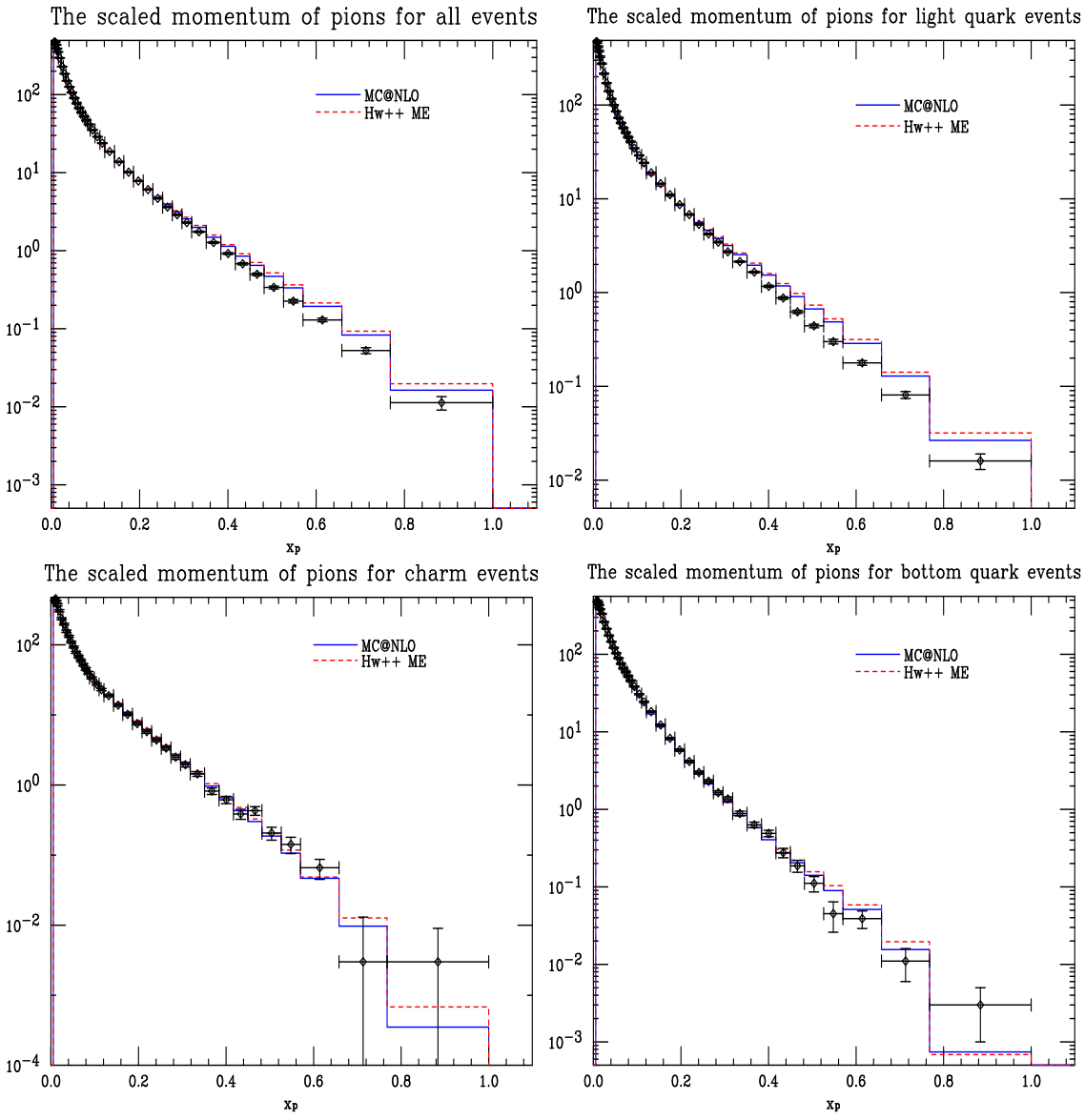

Figure 16: The scaled momentum distributions of pions.

6. Drell-Yan lepton pair production

6.1 Kinematics

The method described above was then applied to Drell-Yan electron pair production at the Tevatron. At leading order, the relevant subprocess is illustrated in Figure 2 is $q + \bar{q} \to V$. The invariant mass Q and the rapidity Y of the boson V can be written in terms of the momentum fractions of the incoming partons, x_q and $x_{\bar{q}}$ as

$$\begin{aligned} Q^2 &= x_q x_{\bar{q}} S \,, \\ Y &= \frac{1}{2} \ln \frac{x_q}{x_{\bar{q}}} \end{aligned} \tag{6.1}$$

where S is the proton-antiproton center-of-mass energy. Inverting this, we have

$$\begin{aligned} x_q &= \sqrt{\frac{Q^2}{S}} e^Y \,, \\ x_{\bar{q}} &= \sqrt{\frac{Q^2}{S}} e^{-Y} \,. \end{aligned} \tag{6.2}$$

Next we consider the real emission subprocesses illustrated in Figure 4. It is convenient to express the kinematics of the NLO diagrams in terms of Mandelstam invariants. For gluon emission, we define

$$\begin{aligned} s &= (p_q + p_{\bar{q}})^2, \\ t &= (p_q - p_g)^2, \\ u &= (p_{\bar{q}} - p_g)^2 \end{aligned} \tag{6.3}$$

with $Q^2 = s + t + u$. For the QCD Compton process, these are given by

$$\begin{aligned} s &= (p_q + p_g)^2, \\ t &= (p_q^{'} - p_g)^2, \\ u &= (p_q - p_q^{'})^2 \,. \end{aligned} \tag{6.4}$$

We can also express the kinematics in terms of the variables x and y which are given by

$$\begin{aligned} x &= \frac{Q^2}{s}; 0 \le x \le 1 \,, \\ y &= \cos\theta; -1 \le y \le 1 \,, \end{aligned} \tag{6.5}$$

where θ is the scattering angle of the emitted parton in the partonic center-of-mass system. Using these definitions, we can show that

$$\begin{aligned} Q^2 &= x x_1 x_2 S \,, \\ Y &= \frac{1}{2} \ln \frac{x_1}{x_2} \frac{2 - (1-x)(1+y)}{2 - (1-x)(1-y)} \end{aligned} \tag{6.6}$$

where x_1, x_2 are now the momentum fractions of the incoming partons in the NLO subprocess and are given in terms of $x_q, x_{\bar{q}}$ by

$$x_1 = \frac{x_q}{\sqrt{x}}\sqrt{\frac{2-(1-x)(1-y)}{2-(1-x)(1+y)}},$$
$$x_2 = \frac{x_{\bar{q}}}{\sqrt{x}}\sqrt{\frac{2-(1-x)(1+y)}{2-(1-x)(1-y)}}. \tag{6.7}$$

At the parton level the Born cross-section for the production of a virtual photon is given by:

$$\sigma_0^i = \frac{4\pi\alpha_{em}^2 e_{q_i}^2}{9Q^2} \tag{6.8}$$

where Q is the electron pair invariant mass. Extending this to the hadronic level, the Born cross-section becomes

$$\frac{d\sigma(S,Q^2)_0^H}{dQ^2} = \int dx_q dx_{\bar{q}} \sum_i \sigma_0^i [f_{q_i/A}(x_{q_i}) f_{q_i/B}(x_{\bar{q}_i}) + q \leftrightarrow \bar{q}] \delta(Q^2 - x_{q_i} x_{\bar{q}_i} S) \tag{6.9}$$

where $f_{q_i/A}(x_{q_i}, Q^2)$ is the distribution function for parton i in the hadron A evaluated at the Born scale, Q.

The differential cross-section for real gluon emission is given by:

$$\frac{d^2\sigma}{\sigma_0 ds dt} = M_{q\bar{q}} = \frac{D_q(x_1) D_{\bar{q}}(x_2)}{D_q(x_q) D_{\bar{q}}(x_{\bar{q}})} \frac{\alpha_S}{2\pi} C_F \frac{Q^2}{s^3 tu} [(s+t)^2 + (s+u)^2] \tag{6.10}$$

where $C_F = 4/3$ and $D_q(x_1) = x_1 f_q(x_1)$ etc. Note that in this and subsequent equations, σ_0 is actually $\frac{d^2\sigma_0}{dQ^2 dY}$. The PDF ratio takes account of the change of kinematics from the Born momentum fractions $x_q, x_{\bar{q}}$ to x_1, x_2. The corresponding differential cross-section for the QCD Compton subprocess is given by

$$\frac{d^2\sigma}{\sigma_0 ds dt} = M_{qg} = \frac{D_q(x_1) D_g(x_2)}{D_q(x_q) D_{\bar{q}}(x_{\bar{q}})} \frac{\alpha_S}{2\pi} T_F \frac{Q^2}{s^4 t} [s^2 + t^2 + 2Q^2 u] \tag{6.11}$$

where $T_F = 1/2$. The shower variables, z and $\tilde{\kappa}$ for the Drell-Yan processes are discussed in detail in [15]. The invariant mass and rapidity of the boson are chosen to be preserved in the definition of the shower variables. Also discussed is the choice of the jet regions (where gluon emission is soft and/or collinear with the parent parton) for the quark q, and antiquark, $\bar{q}$. In terms of the shower variables for the quark jet, the Mandelstam variables become

$$s = \frac{Q^2[1+(1-z)\tilde{\kappa}]}{z},$$
$$t = -Q^2(1-z)\tilde{\kappa},$$
$$u = -(1-z)s \tag{6.12}$$

The jet region is then defined as the area of the $s-t$ phase space where

$$\tilde{\kappa} = \frac{st}{uQ^2} < \tilde{\kappa}_q . \tag{6.13}$$

For the antiquark jet, we have $t \leftrightarrow u$ and thus

$$\tilde{\kappa} = \frac{su}{tQ^2} < \tilde{\kappa}_{\bar{q}} \, . \tag{6.14}$$

In order to ensure that the jet regions touch without overlapping we require $\tilde{\kappa}_q = 1/\tilde{\kappa}_{\bar{q}}$. In the discussion that follows, we choose the symmetrical choice $\tilde{\kappa}_q = \tilde{\kappa}_{\bar{q}} = 1$. The jet and dead regions corresponding to this choice are labeled $J_q, J_{\bar{q}}$ and D respectively in Figure 17. Now the gluon emission probability off the quark in the parton shower approximation

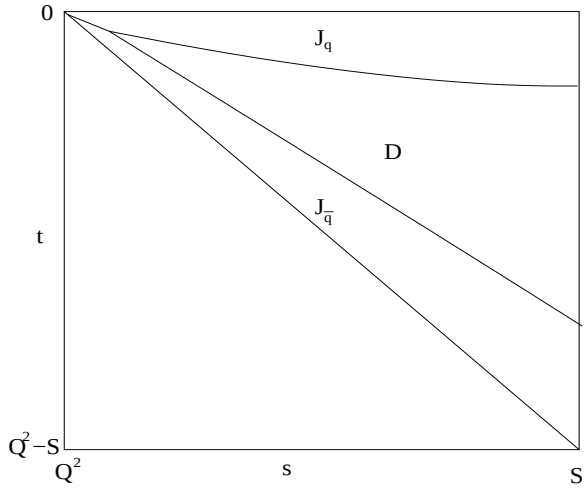

Figure 17: Jet and dead regions in s-t phase space for $q + \bar{q} \to V + g$. Not to scale.

of `Herwig++` is

$$\frac{d^2P}{dzd\tilde{\kappa}} = \frac{\alpha_S}{2\pi} C_F \frac{1+z^2}{\tilde{\kappa}(1-z)} \tag{6.15}$$

which gives a differential cross-section

$$\frac{d^2\sigma}{\sigma_0 ds dt} = M_{C_{q\bar{q}}} = \frac{D_q(x_1) D_{\bar{q}}(x_2)}{D_q(x_q) D_{\bar{q}}(x_{\bar{q}})} \frac{\alpha_S}{2\pi} C_F \frac{(s+u)[s^2 + (s+u)^2]}{s^3 tu} \, . \tag{6.16}$$

Interchange $t \leftrightarrow u$ for the corresponding emission cross-section off the antiquark. Note that the parton shower approximation in (6.16) overestimates the matrix element expression (6.10) and becomes exact in the collinear and soft limit $t \to 0$. For the Compton subprocess $q + g \to V + q$, the parton shower approximation is given by

$$\frac{d^2\sigma}{\sigma_0 ds dt} = M_{C_{qg}} = \frac{D_q(x_1) D_g(x_2)}{D_q(x_q) D_{\bar{q}}(x_{\bar{q}})} \frac{\alpha_S}{2\pi} T_F \frac{(s+u)[u^2 + (s+u)^2]}{s^4 t} \, . \tag{6.17}$$

Interchange $t \leftrightarrow u$ for the subprocess $g + q \to V + q$. In this case there is only one jet region which corresponds to the emitted quark being collinear with the gluon. The same jet definition in (6.13) is used and the corresponding region is shown in Figure 18. Now, we can further re-write the above expressions for the exact differential cross-sections and

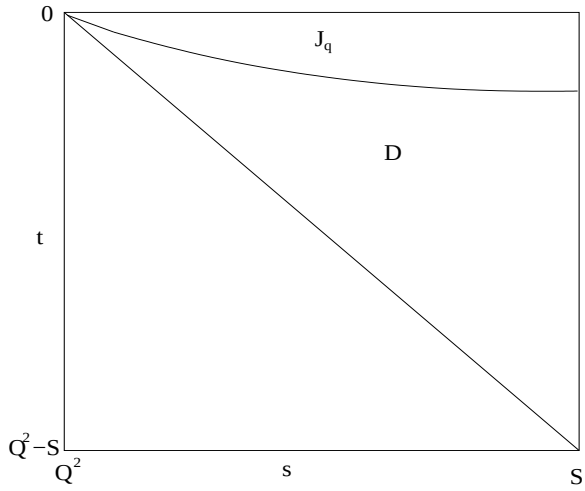

Figure 18: Jet and dead regions in s-t phase space for $q + g \to V + q$. Not to scale.

the parton shower approximation in terms of variables x and y. Using these definitions,

$$t = -\frac{Q^2(1-x)(1-y)}{2x}\,,$$
$$u = -\frac{Q^2(1-x)(1+y)}{2x}\,. \tag{6.18}$$

In these variables the differential cross-sections become

$$M_{q\bar{q}} = \frac{D_q(x_1)D_{\bar{q}}(x_2)}{D_q(x_q)D_{\bar{q}}(x_{\bar{q}})}\frac{\alpha_S}{2\pi}C_F\frac{y^2(1-x)^2+(1+x)^2}{(1-x)(1-y^2)}\,,$$
$$M_{C_{q\bar{q}}} = \frac{D_q(x_1)D_{\bar{q}}(x_2)}{D_q(x_q)D_{\bar{q}}(x_{\bar{q}})}\frac{\alpha_S}{2\pi}C_F\frac{(4+(1-y)^2+2x(1-y^2)+x^2(1+y)^2)(1-y+x(1+y))}{4(1-x)(1-y^2)}\,,$$
$$M_{qg} = \frac{D_q(x_1)D_g(x_2)}{D_q(x_q)D_{\bar{q}}(x_{\bar{q}})}\frac{\alpha_S}{2\pi}T_F\frac{(3+y^2)(1-x)^2-2y(1-x^2)+2(1+x^2)}{4(1-y)}\,,$$
$$M_{C_{qg}} = \frac{D_q(x_1)D_g(x_2)}{D_q(x_q)D_{\bar{q}}(x_{\bar{q}})}\frac{\alpha_S}{2\pi}T_F\frac{1+y^2-2xy(1+y)+x^2(1+y)^2}{x(1-y)}\,. \tag{6.19}$$

Interchange $y \leftrightarrow -y$ in $M_{C_{q\bar{q}}}$ for the antiquark jet and in M_{qg} and $M_{C_{qg}}$ for the process $g + q \to V + q$. The corresponding jet regions of $x - y$ phase space are shown in Figure 19. As we shall see in Section 7, expressing the cross-sections in these variables makes it easier to carry out the MC@NLO subtractions and divergence mappings.

The scale at which the parton distribution functions $D_i(x_1), D_i(x_2)$ are evaluated was set to

$$M = \sqrt{\frac{ut}{s}} \tag{6.20}$$

which in terms of the `Herwig++` variables is given by $\sqrt{(1-z)^2\tilde{\kappa}Q^2}$. This is equal to $\mid \mathbf{k}_\perp \mid$, the transverse momentum of the emitted parton in the partonic center of mass frame. This is the same scale used in the parton shower and is also the scale at which α_S was determined. The Drell-Yan cross-section can be computed in 2 different factorization

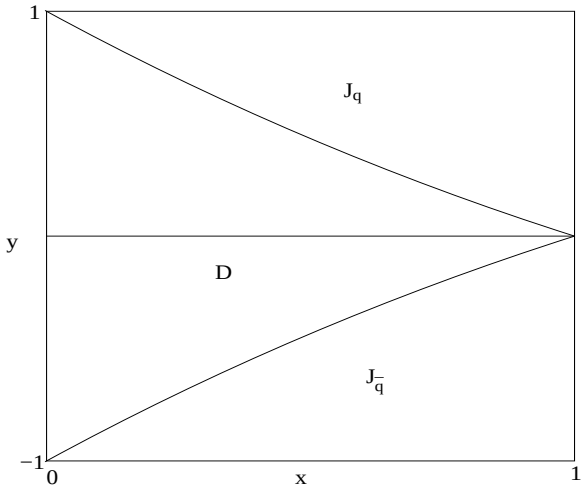

Figure 19: Jet and dead regions in x-y phase space for $q + \bar{q} \to V + g$. Not to scale.

schemes: the DIS scheme and the $\overline{\text{MS}}$ scheme. For comparison, both cross-sections were used for the event generation in this paper. The NLO parton distribution functions were obtained from the CTEQ5d (DIS) and CTEQ5m ($\overline{\text{MS}}$) PDF sets which are frozen at a scale of 1 GeV. For $M < 1$ GeV, $f(x, M)$ was set equal to $f(x, 1)$.

6.2 Next-to-leading order cross-section

In the massless limit, we can integrate the differential cross-section (6.10) for the real emission process $q + \bar{q} \to V + g$ over y using the dimensional regularization scheme to regulate the divergences. The result is [20]

$$\frac{\sigma_R^{NLO}}{\sigma_0} = \frac{\alpha_s}{2\pi} C_F \left(\frac{4\pi}{\mu^2}\right)^{\epsilon} \frac{\Gamma(1-\epsilon)}{\Gamma(1-2\epsilon)} \left[\frac{2}{\epsilon^2}\delta(1-x) - \frac{2}{\epsilon}\frac{1+x^2}{(1-x)_+} + 4(1+x^2)\left(\frac{\ln(1-x)}{1-x}\right)_+ - 2\frac{1+x^2}{1-x}\ln x\right] \tag{6.21}$$

where ϵ is as defined in (2.4) and the plus-prescription is defined by

$$\int_0^1 dx (a(x))_+ b(x) = \int_0^1 a(x)[b(x) - b(1)] \, . \tag{6.22}$$

Now in addition to the real emission diagrams in Figure 4, we have virtual gluon corrections arising from self-energy and vertex corrections. These are illustrated in Figure 20. Integrating these diagrams using dimensional regularization we obtain

$$\frac{\sigma_V^{NLO}}{\sigma_0} = \frac{\alpha_S}{2\pi} C_F \left(\frac{4\pi}{\mu^2}\right)^{\epsilon} \delta(1-x) \frac{\Gamma(1-\epsilon)}{\Gamma(1-2\epsilon)} \left[-\frac{2}{\epsilon^2} - \frac{3}{\epsilon} - 8 + \frac{2}{3}\pi^2\right] \, . \tag{6.23}$$

The product of an infrared and collinear divergence is contained in the $1/\epsilon^2$ term and is cancelled out between the real and virtual diagrams to leave a pure collinear divergence, proportional to $1/\epsilon$. This is cancelled out by QCD corrections to the quark distribution

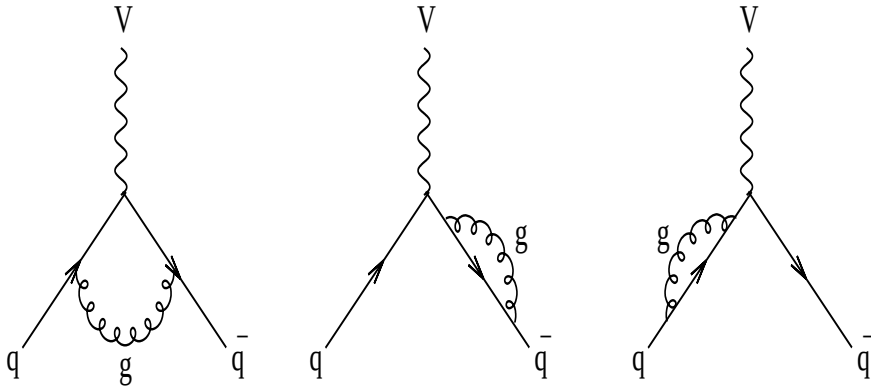

Figure 20: Virtual gluon corrections to the quark-antiquark annihilation Born term $q + \bar{q} \to V$

functions due to real and virtual gluon emission. In the DIS factorization scheme, the NLO distribution function evaluated at a scale μ_F is given in terms of the bare distribution function $f_q^0(x)$ as

$$\begin{aligned} f_q(x,\mu_F^2) &= f_q^0(x) \\ &+ \frac{\alpha_S}{2\pi} C_F \frac{1}{1-\epsilon} \int_x^1 \frac{dw}{w} f_q^0(w) \left[\left(\frac{1+z^2}{(1-z)_+} + \frac{3}{2}\delta(1-z) \right) \left(-\frac{1}{\epsilon} \frac{\Gamma(1-\epsilon)}{\Gamma(1-2\epsilon)} + \ln \frac{\mu_F^2}{4\pi} \right) \right. \\ &+ (1+z^2) \left(\frac{\ln(1-z)}{1-z} \right)_+ - \frac{3}{2} \frac{1}{(1-z)_+} - \frac{1+z^2}{1-z} \ln z \\ &+ \left. 3 + 2z - \left(\frac{9}{2} + \frac{\pi^2}{3} \right) \delta(1-z) \right] \end{aligned} \tag{6.24}$$

where $z = x/w$. Combining these corrections gives the full NLO cross-section ratio [20]

$$\begin{aligned} \frac{\sigma^{NLO}}{\sigma_0} &= \sum_q \int dx_1 dx_2 \frac{x[D_q(x_1,\mu_F^2) D_{\bar{q}}(x_2,\mu_F^2) + q \leftrightarrow \bar{q}]}{D_q(x_q) D_{\bar{q}}(x_{\bar{q}})} \left[\delta(1-x) + \frac{\alpha_S}{2\pi} C_F \left\{ \frac{3}{(1-x)_+} \right. \right. \\ &- 6 - 4x + 2(1+x^2) \left(\frac{\ln(1-x)}{1-x} \right)_+ + \left(1 + \frac{4}{3}\pi^2 \right) \delta(1-x) \\ &+ \left. \left. \left(\frac{1+x^2}{(1-x)_+} + \frac{3}{2}\delta(1-x) \right) 2 \ln \frac{\mu^2}{\mu_F^2} \right\} \right] \end{aligned} \tag{6.25}$$

where $\sum_q$ signifies a sum over parton flavours q. The residual collinear divergence has been cancelled as expected. The last term in the $O(\alpha_S)$ term proportional to $\ln \frac{\mu^2}{\mu_F^2}$ can be eliminated via the DGLAP equation [21, 22, 23, 24] which describes how the distribution functions evolve with the scale μ.

$$\frac{d}{d \ln \mu^2} f_q(x,\mu^2) = \frac{\alpha_S}{4\pi} \int_x^1 \frac{dw}{w} f_q^0(w) P_{qq}\left(\frac{x}{w} \right) \tag{6.26}$$

where the splitting function

$$P_{qq}(z) = C_F \left[\frac{1+z^2}{(1-z)_+} + \frac{3}{2}\delta(1-z) \right] \tag{6.27}$$

describes the probability of a quark coming from the splitting, $q \to qg$. We can use the above expressions to replace $D_q(x, \mu_F^2)$ with $D_q(x, \mu^2)$ in (6.25). The logarithmic term is then cancelled to give

$$\frac{\sigma^{NLO}}{\sigma_0} = \sum_q \int dx_1 dx_2 \frac{x[D_q(x_1,\mu^2)D_{\bar{q}}(x_2,\mu^2) + q \leftrightarrow \bar{q}]}{D_q(x_q)D_{\bar{q}}(x_{\bar{q}})} \left[\delta(1-x) + \frac{\alpha_S}{2\pi} C_F \left\{ \frac{3}{(1-x)_+} \right.\right.$$
$$\left.\left. - \ 6 - 4x + 2(1+x^2)\left(\frac{\ln(1-x)}{1-x}\right)_+ + \left(1 + \frac{4}{3}\pi^2\right)\delta(1-x)\right\}\right] . \tag{6.28}$$

7. MC@NLO method

Now by writing the virtual and PDF corrections in terms of the hard matrix element (6.10), we can rewrite (6.28) in integral from as

$$\frac{\sigma^{NLO}}{\sigma_0} = \sum_q \int dxdy \left[\left\{ \frac{x[D_q(x_1,\mu^2)D_{\bar{q}}(x_2,\mu^2) + q \leftrightarrow \bar{q}]}{D_q(x_q)D_{\bar{q}}(x_{\bar{q}})} \frac{1}{2} \left(\delta(1-x) + \frac{\alpha_S}{2\pi} C_F \left(\frac{3}{(1-x)_+} \right.\right.\right.$$
$$\left.\left.\left. - \ 6 - 4x + 2(1+x^2)\left(\frac{\ln(1-x)}{1-x}\right)_+ + \left(1 + \frac{4}{3}\pi^2\right)\delta(1-x)\right)\right) - M_{q\bar{q}}\right\}$$
$$+ \ M_{q\bar{q}}] \ . \tag{7.1}$$

The first term in the curly brackets is the sum of the Born term, virtual and QCD PDF corrections expressed as an integral over the variables x and y. Since the area of the $x-y$ phase space is 2, there is a factor of $1/2$ in the integrand. The remaining term is the real emission contribution to the cross-section. Now we can define a functional F as in (3.4) which represents final states generated from the 2 different starting configurations; $q + \bar{q} \to V$ and $q + \bar{q} \to V + g$ as

$$\frac{\sigma^{NLO}}{\sigma_0} = \sum_q \int dxdy \left[F_V \left\{ \frac{x[D_q(x_1,\mu^2)D_{\bar{q}}(x_2,\mu^2) + q \leftrightarrow \bar{q}]}{D_q(x_q)D_{\bar{q}}(x_{\bar{q}})} \frac{1}{2} \left(\delta(1-x) + \frac{\alpha_S}{2\pi} C_F \left(\frac{3}{(1-x)_+} \right.\right.\right.$$
$$\left.\left.\left. - \ 6 - 4x + 2(1+x^2)\left(\frac{\ln(1-x)}{1-x}\right)_+ + \left(1 + \frac{4}{3}\pi^2\right)\delta(1-x)\right)\right) - M_{q\bar{q}}\right\}$$
$$+ \ F_{Vg} M_{q\bar{q}}] \ . \tag{7.2}$$

where F_V and F_{Vg} are functionals which represent final states generated from $q + \bar{q} \to V$ and $q + \bar{q} \to V + g$ starting configurations respectively. As discussed in Section 3, this is not entirely correct because of double counting in the final states represented by F_V arising from the parton shower. To resolve this issue, we subtract the contribution from the parton shower contributions, $M_{C_{q\bar{q}}}$ from the integrals in jet regions J_q and $J_{\bar{q}}$ in Figure 19 and integrate the full matrix element $M_{q\bar{q}}$ over the hard emission region, D. The modified

generating functional then becomes

$$
\begin{aligned}
F^{q\bar{q}} = & \sum_q \int_J \Bigg[F_V \left\{ \frac{x[D_q(x_1,\mu^2)D_{\bar{q}}(x_2,\mu^2) + q \leftrightarrow \bar{q}]}{D_q(x_q)D_{\bar{q}}(x_{\bar{q}})} \frac{1}{2} \left(\delta(1-x) + \frac{\alpha_S}{2\pi} C_F \left(\frac{3}{(1-x)_+} \right.\right.\right. \\
& - \left.\left.\left. 6 - 4x + 2(1+x^2) \left(\frac{\ln(1-x)}{1-x} \right)_+ + \left(1 + \frac{4}{3}\pi^2 \right) \delta(1-x) \right) \right) - M_{q\bar{q}} + M_{C_{q\bar{q}}} \right\} \\
& + F_{Vg} \left\{ M_{q\bar{q}} - M_{C_{q\bar{q}}} \right\} \Bigg] \\
& + \sum_q \int_D \Bigg[F_V \left\{ \frac{x[D_q(x_1,\mu^2)D_{\bar{q}}(x_2,\mu^2) + q \leftrightarrow \bar{q}]}{D_q(x_q)D_{\bar{q}}(x_{\bar{q}})} \frac{1}{2} \left(\delta(1-x) + \frac{\alpha_S}{2\pi} C_F \left(\frac{3}{(1-x)_+} \right.\right.\right. \\
& - \left.\left.\left. 6 - 4x + 2(1+x^2) \left(\frac{\ln(1-x)}{1-x} \right)_+ + \left(1 + \frac{4}{3}\pi^2 \right) \delta(1-x) \right) \right) - M_{q\bar{q}} \right\} \\
& + F_{Vg} M_{q\bar{q}} \Bigg] \ . \qquad (7.3)
\end{aligned}
$$

where $J = J_q \cup J_{\bar{q}}$. A similar procedure can be adopted for the Compton subprocess which as discussed has one jet region. In this case the QCD PDF corrections cancel out the collinear divergence in the matrix element. The final result is

$$
\begin{aligned}
F^{qg} = & \sum_q \int_J \Bigg[F_V \left\{ \frac{x[D_q(x_1,\mu^2)D_g(x_2,\mu^2) + q \leftrightarrow g]}{D_q(x_q)D_{\bar{q}}(x_{\bar{q}})} \frac{\alpha_S}{2\pi} T_F \frac{1}{2} \left(\frac{3}{2} - 5x + \frac{9}{2}x^2 \right.\right. \\
& + \left.\left. (x^2 + (1+x^2)) \ln(1-x) \right) - M_{qg} + M_{C_{qg}} \right\} + F_{Vq} \{ M_{qg} - M_{C_{qg}} \} \Bigg] \\
& + \sum_q \int_D \Bigg[F_V \left\{ \frac{x[D_q(x_1,\mu^2)D_g(x_2,\mu^2) + q \leftrightarrow g]}{D_q(x_q)D_{\bar{q}}(x_{\bar{q}})} \frac{\alpha_S}{2\pi} T_F \frac{1}{2} \left(\frac{3}{2} - 5x + \frac{9}{2}x^2 \right.\right. \\
& + \left.\left. (x^2 + (1+x^2)) \ln(1-x) \right) - M_{qg} \right\} + F_{Vq} M_{qg} \Bigg] \qquad (7.4)
\end{aligned}
$$

where $T_F = 1/2$ and F_{Vq} is the functional which represents final states generated from a $q + g \to V + q$ starting configuration. Details of the algorithm used for event generation can be found in Appendix F.

8. Intrinsic p_T

In QCD, the transverse momentum of partons arises in two ways. The first which has been discussed above is due to the real emission of gluons and involves large momentum transfers. This is often termed the perturbative component of the transverse momentum and at large p_T behaves as $1/{p_T}^2$. At low p_T values, with the resummation of the double logarithms from soft gluon emission (as is done in parton shower generators like `Herwig++`), this component of the p_T vanishes as $p_T \to 0$.

The second way in which partons acquire transverse momentum is non-perturbative. It involves small momentum transfers and cannot be calculated by perturbation theory. Therefore this has to be modelled to fit the observed data at low p_T values. A small part of this contribution can be attributed to quarks being confined in the transverse direction to within the radius of the proton and therefore gaining some intrinsic transverse momentum due to the uncertainty principle.

Data on lepton pair transverse momentum from the CFS collaboration [25] suggest that a Gaussian distribution (8.1) best describes the intrinsic p_T distribution.

$$h(p_T) = \frac{2}{{p_{T_{\rm rms}}}^2} e^{\left(-\frac{p_T}{p_{T_{\rm rms}}}\right)^2} \tag{8.1}$$

where $p_{T_{\rm rms}}$ is the root-mean-square p_T of the Gaussian distribution.

The intrinsic p_T (8.1) was implemented in `Herwig++`. The intrinsic p_T component is generated according to the distribution using a random number generator and added to the parent partons obtained at the end of the space-like shower originating from the hard QCD process.

Figure 21 shows the distribution of the χ^2 per degree of freedom obtained for different $p_{T_{\rm rms}}$ fits to run I (1800 GeV) CDF data [26] for Drell-Yan Z boson production and the best fit value can be seen to be $p_{T_{\rm rms}} = 2.1$ GeV.

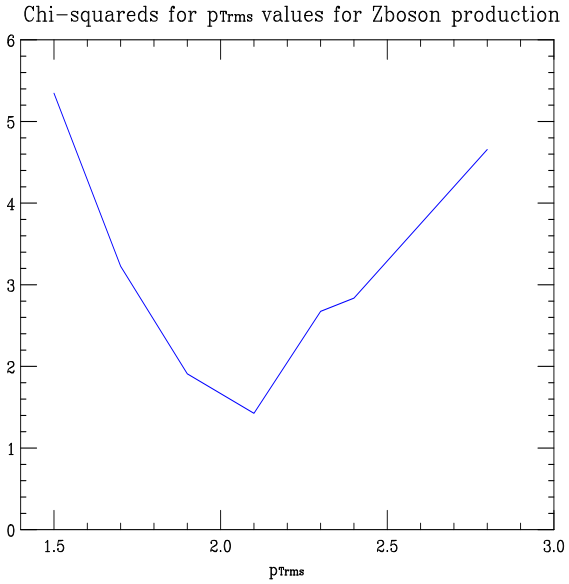

Figure 21: χ^2 per degree of freedom.

9. Results on Drell-Yan production

Details of event generation and partonic final state properties are described in Appendices E, F and G. Once generated the events were showered using `Herwig++` version 2.0.1 and the distribution of the transverse momentum of the Z boson was obtained. The hadronization scale was set to the default value of 0.631 GeV and the 2-loop α_S value was used. Figure

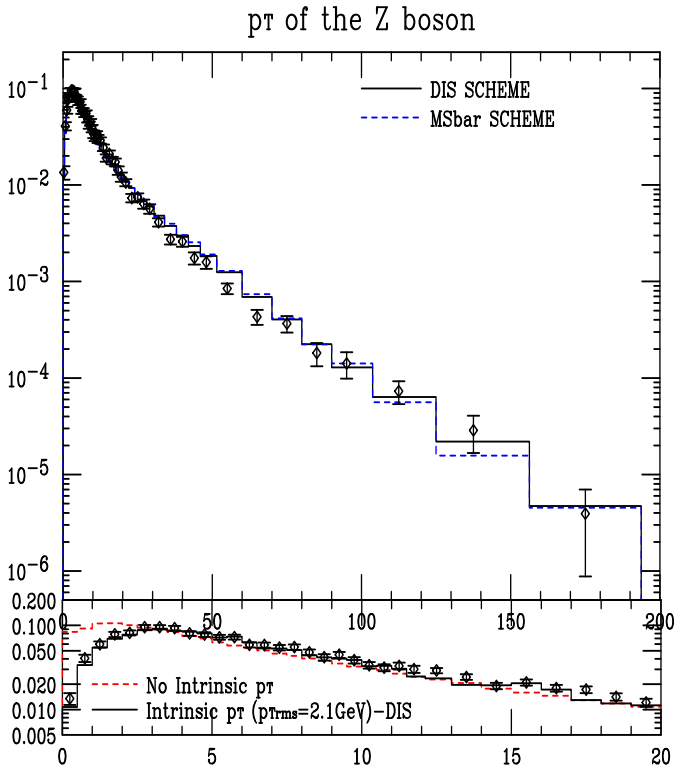

Figure 22: Transverse momentum of the Z boson. Data from [26].

22 shows a comparison of the distributions obtained for both factorization schemes with CDF Run I data [26].

Also shown in Figure 23 are the rapidity distributions of the Z boson and the positively charged lepton arising from its decay. for comparison distributions are compared against Run II ($\sqrt{s} = 1.96$ TeV) data from the D0 collaboration [27].

As can be seen in Figure 22 the MC@NLO method provides a good description of the CDF data for the transverse momentum of the Z boson. It also proves to be stable with respect to change of scheme. Figure 22 also shows the effect of the p_T distribution in the low p_T region. The red dashed line corresponds to setting $p_{T_{\rm rms}} = 0$ GeV whilst the black line corresponds to setting $p_{T_{\rm rms}} = 2.1$ GeV. Comparing the two, one can see the effect of adding the non-perturbative intrinsic p_T to the parton shower which gives a better description of the data.

In addition, Figure 23 shows that the predicted rapidity distributions of the Z boson and the positive lepton produced are stable with respect to the change of scheme.

10. Summary and conclusions

We have successfully applied the MC@NLO method to e^+e^- annihilation and Drell-Yan processes modelled by the `Herwig++` event generator. In general, we conclude that the MC@NLO method provides an improved description of event shape distributions when

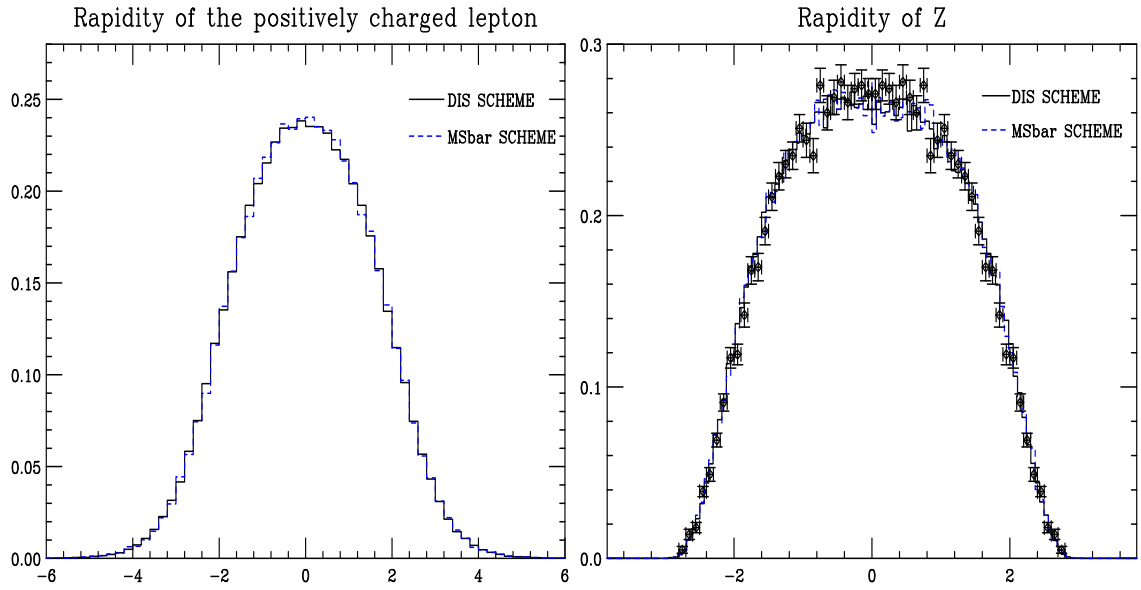

Figure 23: Rapidity distributions of the positively charged lepton and the Z boson.

compared to pure leading order Monte Carlo results. As we have seen, the MC@NLO results for e^+e^- annihilation do not differ greatly from the matrix element correction results although we are now confident that the results are normalised to the full NLO cross-section. Better results were obtained using the positive weight Nason@NLO method where the hardest gluon emission was generated first [5]. The MC@NLO method applied to the Drell-Yan process gives a good description of the transverse momentum and stable predictions for Z boson and lepton. The differences between the performance of the method for e^+e^- annihilation and Drell-Yan production may be attributed to the different shower variables for initial state and final state radiation.

In addition, we have also successfully implemented the intrinsic p_T component for hadron-hadron collisions into `Herwig++`.

11. Acknowledgements

I am grateful to the other members of the `Herwig++` collaboration for developing the program that underlies the present work and for helpful comments. I am particularly grateful to Bryan Webber for constructive comments and discussions throughout.

A. Monte Carlo algorithm for e^+e^- annihilation

The integrals in (3.15) can be evaluated using a variety of Monte Carlo methods. In this report, the 'Hit or Miss' Monte Carlo method is used. This is the simplest and oldest form

of Monte Carlo integration and essentially involves finding the area of a region in phase space by integrating over a larger region, a binary function which is 1 in the region and 0 elsewhere. The sampling method used for the points $x_q, x_{\bar{q}}$ is the importance sampling method whereby more samples are taken from regions where the integrand is large and less from regions where it is small. This ensures that the sampled points have the same distribution as the integrand.

First, let us investigate what each of the terms in (3.15) signify. The program `Herwig++` generates n-jets from an inputed set of n momentum space points $(x_i, \ldots, x_n)$. So for 2 and 3-jet formation, we require sets of 2 and 3 momentum space points with each set corresponding to an event in the phase space. The relative numbers of these events as well as the x_i values can be obtained from (3.15) as outlined. (2-jet events have $x_q, x_{\bar{q}} = 1$). In the discussion that follows, $\sqrt{s}$ was set to $M_Z = 91.2$ GeV and $\alpha_S(M_z) = 0.118$.

1. Randomly sample points $x_q, x_{\bar{q}}$, in each of regions $J_q, J_{\bar{q}}$ and D of the phase space and using the "Hit Or Miss" Monte Carlo method, evaluate the 4 integrals, $I_J^{(2)}, I_J^{(3)}, I_D^{(2)}$ and $I_D^{(3)}$ as well as their absolute sum, I.

$$\begin{aligned}
I_J^{(2)} &= \int_J dx_q dx_{\bar{q}} \left[2 - \frac{\alpha_S}{2\pi} C_F \left\{M - M_C - 3\right\}\right] , \\
I_J^{(3)} &= \int_J dx_q dx_{\bar{q}} \frac{\alpha_S}{2\pi} C_F [M - M_C] , \\
I_D^{(2)} &= \int_D dx_q dx_{\bar{q}} \left[2 - \frac{\alpha_S}{2\pi} C_F \left\{M - 3\right\}\right] , \\
I_D^{(3)} &= \int_D dx_q dx_{\bar{q}} \frac{\alpha_S}{2\pi} C_F M , \\
I &= \mid I_J^{(2)} \mid + \mid I_J^{(3)} \mid + \mid I_D^{(2)} \mid + \mid I_D^{(3)} \mid \ . \qquad \text{(A.1)}
\end{aligned}$$

   Note also the maximum values of the integrands in $I_J^{(3)}$ and $I_D^{(3)}$.

2. The eventual proportion of 2-jet Monte Carlo events will be determined by the ratio $\frac{|I_J^{(2)}| + |I_D^{(2)}|}{I}$. Likewise, the proportions of 3-jet events in the soft regions $J_q, J_{\bar{q}}$ and the hard region D are determined by the ratios $\frac{|I_J^{(3)}|}{I}$ and $\frac{|I_D^{(3)}|}{I}$ respectively. The algorithm below is then used to importance-sample the 3-jet events so that the corresponding $(x_q, x_{\bar{q}})$ values of the Monte Carlo events have the same distribution as the integrands in $I_J^{(3)}$ and $I_D^{(3)}$:

   (a) For event generation in region R ($R = D, J_q$ or $J_{\bar{q}}$), randomly select a point $x_q, x_{\bar{q}}$ in that region.

   (b) Evaluate the absolute value of the integrand in $I_R^{(3)}$ for this point, $\mid w(x_q, x_{\bar{q}}) \mid$. Is $\mid w(x_q, x_{\bar{q}}) \mid > R \mid w_{\max} \mid$? (R is a random number between 0 and 1 and $\mid w_{\max} \mid$ is the maximum value of $\mid w(x_q, x_{\bar{q}}) \mid$ determined in Step 1).

(c) If NO, return to (a). If YES, accept the event and set $w^{\rm unw}$= sgn $w(x_q, x_{\bar{q}})$ i.e. $w^{\rm unw} = 1$ if $w(x_q, x_{\bar{q}})$ is positive and -1 if negative. (In regions J_q and $J_{\bar{q}}$, $M < M_C$, hence the integrands and the integral, $I_J^{(3)}$ in these regions are negative). This process is called `unweighting`.

(d) Repeat the process until the correct proportion of 2-jet and 3-jet events have been generated.

(e) Using the importance-sampled points, obtain an estimate for the integral, $I_R^{(2,3)} = \frac{\sum w^{\rm unw}}{N} \times I$, where N is the total number of Monte Carlo events generated. We typically use $N = 10^6$.

This method of generating Monte Carlo events is termed 'Monte Carlo at Next to Leading Order' or MC@NLO. In this way, for a total of N events, the correct proportion of 2-jet and 3-jet events with $\pm$ unit weight is generated with the same distribution as the integrands in (A.1). All of these integrals are finite, but the integrands are divergent at isolated points within the integration regions. Before the sampling could be carried out, the divergences in the integrands (which cause problems in the sampling process) had to be taken care of. This is the described in section B.

B. Divergences and mappings for e^+e^- annihilation

B.1 Divergences in dead region D

In region D, the hard matrix element:

$$M(x_q, x_{\bar{q}}) = \frac{x_q^2 + x_{\bar{q}}^2}{(1 - x_q)(1 - x_{\bar{q}})} \tag{B.1}$$

diverges as $(x_q, x_{\bar{q}}) \to (1, 0), (0, 1)$ and $(1, 1)$. To avoid these divergences, one can map the divergent regions into another region in such a way that the divergence is regularized. This is ensured by the fact that the region of integration vanishes as the singularity is approached. The mappings used are presented.

B.1.1 Region D : $(1, 1)$

There is a double pole in M at $(x_q, x_{\bar{q}}) = (1, 1)$. To avoid this pole, the region $x_q, x_{\bar{q}} > \frac{3}{4}$ is mapped into a region which includes D but whose width vanishes quadratically as $x_q, x_{\bar{q}} \to 1$ [15]. The mapping used is:

$$\begin{aligned} x_q^{'} &= 1 - \left[\frac{1}{4} - (1 - x_q)\right] = \frac{7}{4} - x_q \,, \\ x_{\bar{q}}^{'} &= 1 - 2(1 - x_q^{'}) \left[\frac{3}{4} - (1 - x_{\bar{q}})\right] = \frac{5}{8} + \frac{1}{2}x_q + \frac{3}{2}x_{\bar{q}} - 2x_q x_{\bar{q}} \end{aligned} \tag{B.2}$$

when $x_q > x_{\bar{q}} > \frac{3}{4}$. This mapping also introduces an extra weight factor of $2(1 - x_q^{'})$ in the integrand. (Interchange x_q and $x_{\bar{q}}$ in both the mapping and weight factor when $x_{\bar{q}} > x_q > \frac{3}{4}$). Figure 24 shows the region mapped (solid) and the region mapped onto (dashed).

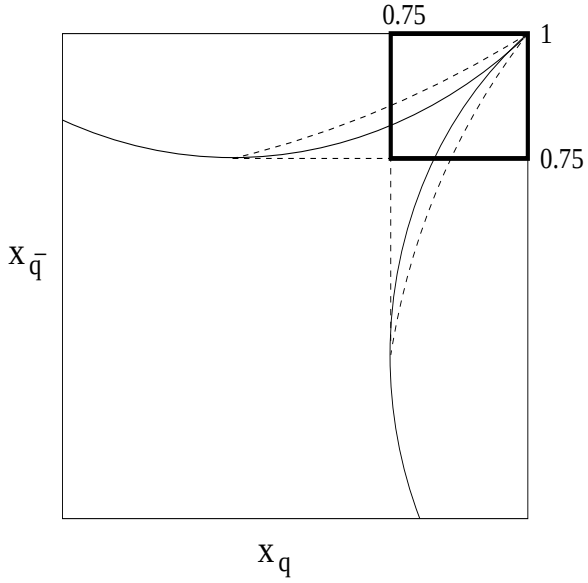

Figure 24: The mapped region (solid) and the region mapped onto (dashed)

B.1.2 Region D : $(1,0),(0,1)$

A simple pole is approached in M as $(x_q, x_{\bar{q}}) \to (1,0)$ and $(0,1)$. In the region $x_q < \frac{5}{8}$, $x_{\bar{q}} > \frac{3}{4}$, a new set of random points is generated for points which fall between the lines $x_q = 2.5(1 - x_{\bar{q}})$ and $x_q = 1 - x_{\bar{q}}$. These points have an extra weight factor to cancel the divergence as the pole is approached. The mapping used is:

$$\begin{aligned} x_{\bar{q}}^{'} &= 1 - 0.25 r_2 \,, \\ x_q^{'} &= (1 + 1.5 r_1)(1 - x_{\bar{q}}^{'}) \end{aligned} \tag{B.3}$$

where r_1 and r_2 are random numbers in the range $[0,1]$. This mapping introduces a weight factor of $2r_2$ in the integrand. Interchange x_q and $x_{\bar{q}}$ in the mapping for the region where $x_{\bar{q}} < \frac{5}{8}, x_q > \frac{3}{4}$. The mapped regions are shown with solid boundaries in Figure 25.

B.2 Divergences in jet regions J_q and $J_{\bar{q}}$

In both regions J_q and $J_{\bar{q}}$, there is a simple pole in the term $(M - M_C)$ at $(x_q, x_{\bar{q}}) = (1,1)$. In the region $x_q, x_{\bar{q}} > \frac{3}{4}$, a new set of random points are generated which have a weight factor to cancel the divergence. The mapping used in region J_q where $x_{\bar{q}} > x_q$ is:

$$\begin{aligned} x_q^{'} &= 1 - 0.25 r_1 \,, \\ x_{\bar{q}}^{'} &= 1 - (1 - x_q^{'}) r_2 \end{aligned} \tag{B.4}$$

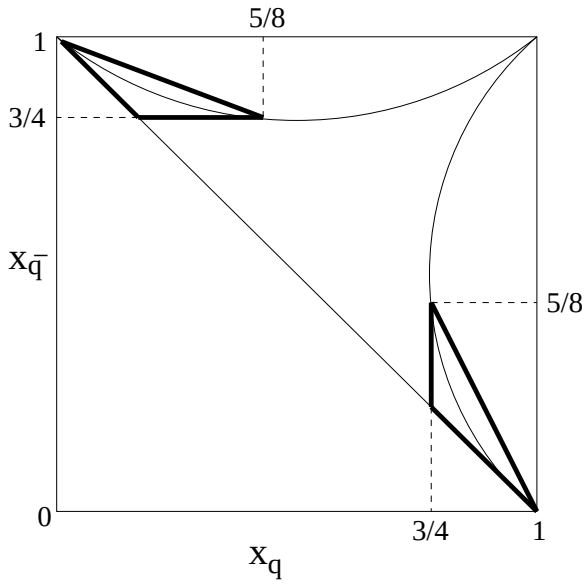

Figure 25: Mapped regions

where r_1 and r_2 are random numbers in the range $[0, 1]$. The weight factor for this mapping is $2r_1$. For region $J_{\bar{q}}$, where $x_q > x_{\bar{q}}$, interchange x_q and $x_{\bar{q}}$ in the mapping. The mapped regions are shown with solid boundaries in Figure 26. There are no poles at (1,0) and (0,1)

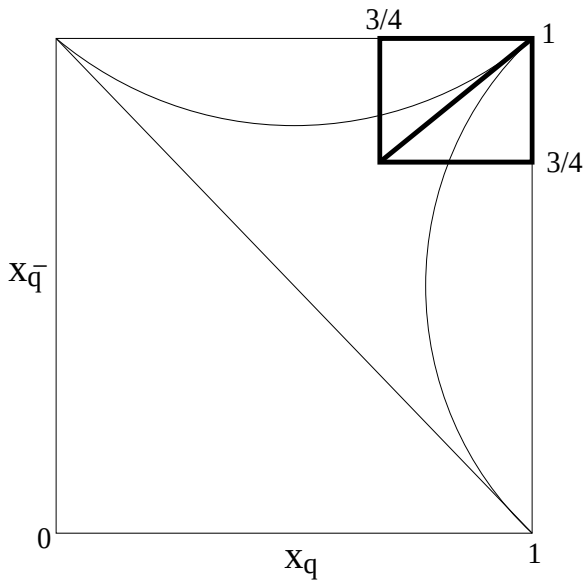

Figure 26: Mapped regions

because at these points the singularities in M and M_C are cancelled out in the subtraction.

B.3 Mapping method

To illustrate the method behind determining the mappings, the mapping in section B.1.2 will be explicitly calculated here. Figure 25 shows the mapped region which is between the lines $x_{\bar{q}} = 2.5(1 - x_q)$ and $x_{\bar{q}} = 1 - x_q$. The integrand in this region goes as $\frac{1}{1-x_{\bar{q}}}$ and hence is divergent as $x_{\bar{q}} \to 1$. By performing the change of variables shown in (B.5), this divergence can be regularized.

$$\begin{aligned} &\int_{0.75}^{1} dx_{\bar{q}} \int_{1-x_{\bar{q}}}^{2.5(1-x_{\bar{q}})} dx_q f(x_q, x_{\bar{q}}) \\ &= \int_0^1 dr_2 \int_0^1 dr_1 (0.25^2 \times 1.5 r_2) f(x_{\bar{q}} = 1 - 0.25 r_2, x_q = (1 + 1.5 r_1)(1 - x_{\bar{q}})) \ . \end{aligned} \tag{B.5}$$

r_1 and r_2 are random numbers between $[0, 1]$ as discussed in section B.1.2 and the factor $0.25^2 \times 1.5 r_2$ is the Jacobian factor arising from the change of variables. It can be seen that this Jacobian factor explicitly removes the $\frac{1}{1-x_{\bar{q}}}$ divergence in the integrand. Since the 'Hit Or Miss' Monte Carlo method is used to perform the integration, the weights of points in the mapped region must be multiplied by an area factor equal to inverse of the area of the mapped region i.e. $\frac{64}{3}$ in this case. Hence the weight of a sampled point in this region is

$$0.25^2 \times 1.5 r_2 \times \frac{64}{3} \times f = 2 r_2 f \ . \tag{B.6}$$

A similar treatment is followed for all the other divergences. Now that we have taken care of the divergences, we need to check that the mappings give the true value of the integral.

B.4 Testing the mappings

The integration package `VEGAS` [28] was used to obtain estimates for the integrals in (3.15). `VEGAS` is an iterative and adaptive Monte Carlo integration algorithm which is based on importance sampling and is good for the evaluation of multidimensional integrals.

The algorithm was used to compute integrals $I_J^{(3)}$ and $I_D^{(3)}$ in section A. Forty iterations were carried out with 10^7 program calls per iteration. The results are compared with the values obtained with the mappings and unweighting procedure described in sections 3 and B. Also worth comparing are the integrals obtained before the unweighting in step 2 of section A. This gives a measure of how efficient the unweighting process is. These are presented in the Table 1. The errors in the `VEGAS` results are not to be trusted as they appear to be underestimated.

The estimated value for the ratio, $\frac{\sigma_{\text{total}}}{\sigma_0}$ after the mappings can also be compared with the true value, $[1 + \frac{\alpha_S}{\pi}]$ to $O(\alpha_S)$. This ratio is the sum of the four integrals, $I_J^{(2)}, I_J^{(3)}, I_D^{(2)}$ and $I_D^{(3)}$ outlined in section A. Table 3 shows the relative number of 2-jet and 3-jet events generated from a total of 10^6 events.

INTEGRAL	$I_J^{(3)}$	$I_D^{(3)}$
With mappings	$-0.0393 \pm 1 \times 10^{-4}$	$0.0339 \pm 1 \times 10^{-4}$
VEGAS	$-0.03923063 \pm 6 \times 10^{-8}$	$0.0339753 \pm 9 \times 10^{-7}$
Unweighted events	$-0.0393 \pm 1 \times 10^{-4}$	$0.0339 \pm 1 \times 10^{-4}$

Table 1: Comparison of VEGAS with weighted and mapping integrals

True cross-section ratio	Estimated cross-section ratio
1.0375	$1.0367 \pm 1.3 \times 10^{-3}$

Table 2: Comparison of the cross-section ratio with the true cross-section ratio to $O(\alpha_S)$

Number of 2-jet events	Number of 3-jet events
934,567	65,433

Table 3: Relative number of 2-jet and 3-jet events per 1,000,000 events

C. Heavy quark integrals

Event generation for heavy quark production follows the same lines as discussed in Section A for the massless case and the soft divergence mappings used are also implemented in the heavy parton case. 10^7 events were generated in this way to obtain a better estimate of the cross-section. The 3-jet integrals obtained are presented in Tables 4 and 5 for both charm and bottom quark production from vector boson exchange. The VEGAS results are also presented for comparison. The maximum absolute weights in the two regions J and D are also presented.

Integral	$I_J^{(3)}$	$I_D^{(3)}$
With mappings	$-0.0403 \pm 3 \times 10^{-4}$	$0.03215 \pm 4 \times 10^{-5}$
VEGAS	$-0.03989509 \pm 7 \times 10^{-8}$	$0.0321728 \pm 7 \times 10^{-7}$
Maximum |weight|	2360	15

Table 4: Comparison of VEGAS and mapping integrals for charm quarks

Integral	$I_J^{(3)}$	$I_D^{(3)}$
With mappings	$-0.0483 \pm 2 \times 10^{-3}$	$0.02809 \pm 2 \times 10^{-3}$
VEGAS	$-0.0459681 \pm 6 \times 10^{-7}$	$0.0281315 \pm 1 \times 10^{-7}$
Maximum |weight|	13338	9.3

Table 5: Comparison of VEGAS and mapping integrals for bottom quarks

$I_J^{(3)}$ and $I_D^{(3)}$ here are the corresponding heavy parton integrals to the integrals $I_J^{(3)}$ and $I_D^{(3)}$ discussed in section A in the massless limit. The estimated value for the ratio, $\frac{\sigma_{total}}{\sigma_V}$

after the mappings can also be compared with the true value at $O(\alpha_S)$, $1 + c_1 \frac{\alpha_S}{\pi}$.

Quark flavour	True ratio	Estimated ratio
Charm	1.0373	$1.0374 \pm 6 \times 10^{-4}$
Bottom	1.0385	$1.0387 \pm 3 \times 10^{-3}$

Table 6: Comparison of the cross-section ratio with the true cross-section ratio to $O(\alpha_S)$

The problem with this method arises during the unweighting process described in Section A. The efficiency of the unweighting process for a particular can be defined as the ratio of the integral over the region to the maximum value of its integrand $\frac{I}{w_{\max}}$. This is a measure of the rejection rate in the unweighting process. So the smaller the value of $w_{\max}$, the greater the unweighting efficiency. Now, the divergence mappings described in section B.2 are not as effective in smoothing out the distribution of event weights in regions J_Q and $J_{\bar{Q}}$ (where there is a soft gluon singularity) as was the case in the massless limit. This results in a relatively peaked distribution in the soft gluon region and hence a relatively large absolute value for the maximum weight (see Tables 4 and 5). Due to this, the unweighting process is comparatively inefficient.

To resolve this, we can impose a limit on the gluon 'softness' allowed in 3-jet events from the soft and collinear regions, J_Q and $J_{\bar{Q}}$. 3-jet events with gluon energy fractions, x_g below this limit are then considered to be 2-jet events with x_Q and $x_{\bar{Q}}$ equal to 1 and $x_g = 0$. For charm and bottom quarks, a limiting value of 1×10^{-4} was chosen such that the maximum absolute weight is sufficiently lowered (giving a smoother distribution) whilst the estimated cross-section is not too far off from the true cross-section (Table 7). The same method was applied for the axial vector boson coupling.

D. Assigning parton properties

Having chosen a phase space point, to generate a full event we have to assign full 4-momenta, as well as flavour, spin and colour information to the partons. In this section we address these issues in turn.

D.1 Momentum 4-vectors

Figure 27 shows the production of a quark of 4-momentum p_1, an antiquark of 4-momentum p_2 and a gluon of 4-momentum p_3 from an e^+e^- annihilation reaction in the centre-of-mass frame. It can be shown that the angles θ_{ij} between partons of momenta p_i and p_j satisfy

Quark flavour	Maximum 'soft' |weight|	Estimated ratio
Charm	4.8	$1.0381 \pm 5 \times 10^{-4}$
Bottom	43.1	$1.0439 \pm 2 \times 10^{-3}$

Table 7: Cross-section ratio and maximum weights after phase-space cut-offs

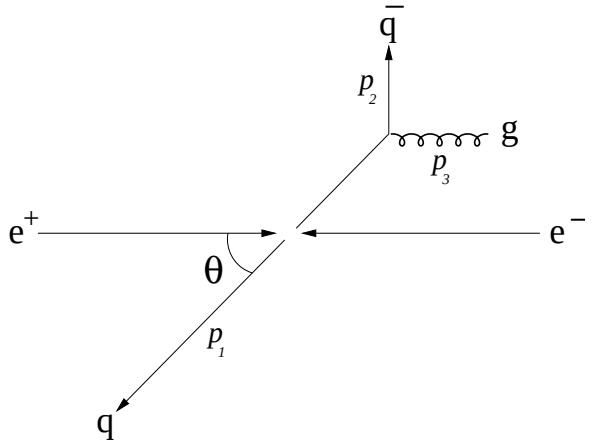

Figure 27: Annihilation in centre-of-mass frame

the relations,

$$\begin{aligned}
\cos\theta_{12} &= \frac{x_q x_{\bar{q}} - 2(1-x_g) + 4\rho}{\sqrt{(x_q^2 - 4\rho)(x_{\bar{q}}^2 - 4\rho)}}\,, \\
\cos\theta_{13} &= \frac{x_q x_g - 2(1-x_{\bar{q}})}{x_g\sqrt{x_q^2 - 4\rho}}\,, \\
\cos\theta_{23} &= \frac{x_{\bar{q}} x_g - 2(1-x_q)}{x_g\sqrt{x_{\bar{q}}^2 - 4\rho}}\,.
\end{aligned} \tag{D.1}$$

The angular differential cross-section for the process $e^+e^- \to q\bar{q}$ is defined in (D.2) [17]. This is the distribution of the angle Θ between the initial $q\bar{q}$ axis (before gluon emission) and the e^+e^- axis.

$$\frac{d\sigma}{d\cos\Theta} = (1+\cos^2\Theta)\sigma_U + 2\sin^2\Theta\sigma_L + 2\cos\Theta\sigma_F\,. \tag{D.2}$$

In the Born approximation,

$$\begin{aligned}
\sigma_U &= \beta\sigma_{VV} + \beta^3\sigma_{AA}\,, \\
\sigma_L &= \frac{1}{2}(1-\beta^2)\beta\sigma_{VV}\,, \\
\sigma_F &= \beta^2\sigma_{VA}
\end{aligned} \tag{D.3}$$

with

$$\begin{aligned}
\sigma_{VV} &= \frac{\pi\alpha^2}{2s}\left[Q_f^2 - 2Q_f V_e V_f \chi_1(s) + (A_e^2 + V_e^2)V_f^2 \chi_2(s)\right] , \\
\sigma_{AA} &= \frac{\pi\alpha^2}{2s}\left[(A_e^2 + V_e^2)A_f^2 \chi_2(s)\right] , \\
\sigma_{VA} &= \frac{\pi\alpha^2}{2s}\left[-2Q_f A_e A_f \chi_1(s) + 4A_e V_e A_f V_f \chi_2(s)\right] , \\
\beta &= \sqrt{1-4\rho}\,, \\
\chi_1(s) &= \delta\frac{s(s-M_Z^2)}{(s-M_Z^2)^2 + \Gamma_Z^2 M_Z^2}\,, \\
\chi_2(s) &= \delta^2\frac{s^2}{(s-M_Z^2)^2 + \Gamma_Z^2 M_Z^2}\,, \\
\delta &= \frac{\sqrt{2}G_F M_Z^2}{4\pi\alpha}\ ,
\end{aligned} \tag{D.4}$$

G_F is the Fermi constant, α is the electromagnetic coupling, M_Z and Γ_Z are the mass and total decay width of the Z boson respectively and V_f and A_f are the vector and axial couplings of fermion, f to the Z boson.

By applying the unweighting procedure described in step 2 of section A to (D.2), the angles Θ for each event can be distributed according to angular differential cross-section. Since the azimuthal angles for $q\bar{q}$ production and the $q \to qg$ process are isotropic, 4-momentum vectors for the quark, antiquark and gluon can therefore straightforwardly be constructed for each event.

Initially all parton 4-momenta were generated in the massless limit. Though this is not essential for the parton shower, the parton 3-momenta were rescaled by a common factor using the Newton-Raphson iteration method to give the right parton masses (for heavy partons) and a gluon virtuality of 0.75 GeV.

D.2 Flavour

To assign flavour to the quarks, we need to investigate the flavour dependence of the total cross-section for $e^+e^- \to q\bar{q}$. Integrating (D.2) over all angles Θ gives;

$$\sigma_f = (\beta + \frac{1}{2}\beta(1-\beta^2))\sigma_{VV} + \beta^3\sigma_{AA}\ . \tag{D.5}$$

σ_f is the contribution of a quark of flavour f to the total cross-section. Hence the quarks are assigned flavours according to the relative values of σ_f.

D.3 Spins

To assign spins to the partons, the matrix element for $e^+e^- \to q\bar{q}$ is calculated for all possible helicity configurations and its modulus squared is used as a weight in allocating spins to the quarks and antiquarks. In other words, the helicity configurations are allocated according to their contributions to the total cross-section. It is assumed that the electron and positron beams are unpolarised so that the helicities of the electrons and positrons are assigned randomly.

In the massless limit, the chiral components are the helicity eigenstates and so when a Z boson (which couples to chiral components) is exchanged, the matrix elements for different spin configurations are straightforward to calculate. In the heavy parton case, the chiral components are a mixture of helicity eigenstates so that the matrix element calculations become more complicated. Also, there are 4 possible helicity configurations in the massless limit whilst there are 8 helicity configurations in the heavy parton case (electrons and positrons are assumed to be massless).

As an illustration, the matrix element for the helicity configuration, $e^-_\uparrow\ e^+_\downarrow\ q_\uparrow\ \bar{q}_\downarrow$ is given in (D.6).

$$\begin{aligned} M_{\uparrow\downarrow\uparrow\downarrow} = (1+\cos\Theta)^2 &\left[{c^e_{\mathrm{R}}}^2 \chi_2 \lambda^2 \left[c^q_{\mathrm{L}} \left(\frac{\sqrt{s}}{2} - p_{\mathrm{cm}} \right) + c^q_{\mathrm{R}} \left(\frac{\sqrt{s}}{2} + p_{\mathrm{cm}} \right) \right]^2 \right. \\ - \ 2eQ_q c^e_{\mathrm{R}} \chi_1 \lambda &\left. \left[c^q_{\mathrm{L}} \left(\frac{\sqrt{s}}{2} - p_{\mathrm{cm}} \right) + c^q_{\mathrm{R}} \left(\frac{\sqrt{s}}{2} + p_{\mathrm{cm}} \right) \right] + e^2 Q_q^2 \right] \end{aligned} \tag{D.6}$$

where

$$\lambda^2 = \frac{2\sqrt{32}\pi\alpha}{s}\,, \tag{D.7}$$

c^q_R, c^q_L, c^e_R and c^e_L are the right and left-handed couplings of the quarks and leptons to the Z boson respectively and p_{cm} is the centre-of-mass momentum of the quark.

So far we have assigned the particles into helicity eigenstates. This is because the interface of the event record to the event generator `Herwig++`, requires that the electrons, positrons and partons are in definite helicity eigenstates. In practice however, for an unpolarised beam of electrons and positrons, the spins of the partons resulting from the annihilation reaction are superpositions of the helicity eigenstates. The spin density matrix, ρ for spin-$\frac{1}{2}$ particles is given by;

$$\rho = \frac{1}{2}[I + \langle\sigma\rangle \cdot \sigma] \tag{D.8}$$

which can be written as

$$\begin{bmatrix} \frac{1}{2}(1+a_1) & \frac{1}{2}(a_2 - ia_3) \\ \frac{1}{2}(a_2 + ia_3) & \frac{1}{2}(1-a_1) \end{bmatrix} \tag{D.9}$$

where $\langle\sigma\rangle$ is the matrix of spin expectation values, $\sigma = (\sigma_x, \sigma_y, \sigma_z)$ which are the Pauli matrices and $\frac{1}{2}a_1, \frac{1}{2}a_2$ and $\frac{1}{2}a_3$ are the expectation values of the spin matrices S_z, S_x, S_y respectively. Since the helicity eigenstates are also eigenstates of S_z (taking the z axis to be along the quark momentum direction) and since $\frac{1}{2}(1+a_1)$ and $\frac{1}{2}(1-a_1)$ are the probabilities of a parton being in either state, we can assign spin states to the partons by distributing values of a_1 between 0 and 1 according to their corresponding matrix element contributions.

D.4 Gluon emission

For the 3-jet events, the gluon can be radiated either from the quark or anti-quark. Intuitively, we expect the fastest or more energetic of the two partons to be the least likely

to radiate the gluon i.e. most likely to keep its original direction. In the massless limit, it has been shown that the relative probabilities of a parton retaining its direction after production (not emitting the gluon) are in the ratio of their respective energies squared. i.e $\propto x_i^2$ [29]. This notion is used to assign mother partons to the gluons in the 3-jet events. (For heavy quarks, this procedure is approximate). In addition it can be shown that the helicity of the gluon equals the non-emitting parton's helicity which is opposite to the spin of the mother parton [29].

D.5 Colour

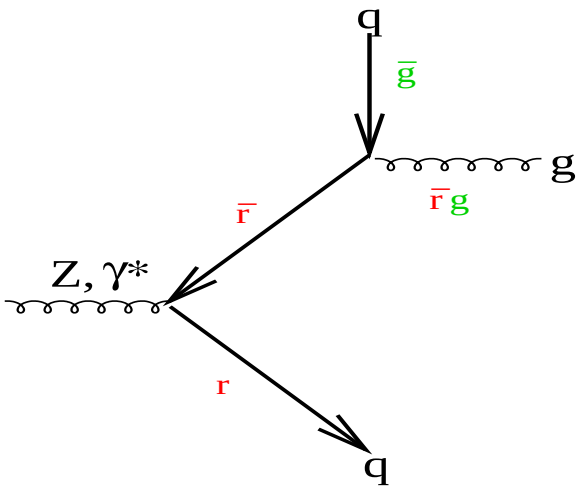

Figure 28: Colour Flow

The colour of a parton flows out of its production vertex whilst its anticolour flows into its production vertex. The gluon carries the anticolour of the quark colour and the colour corresponding to the antiquark anticolour. This is illustrated in Figure 28 for the specific case where a $\bar{r}$ antiquark radiates a $g\bar{r}$ gluon and becoming a $\bar{g}$ antiquark in the process. (The colour flow lines are essentially the same for a radiating quark).

Colours were assigned to the partons taking into account the restrictions on the colour flow discussed above. Note that this colour treatment is the planar approximation, which is correct only to $O(\frac{1}{{N_C}^2})$ where $N_C = 3$ is the number of colours. In this approximation, it is always possible to draw any Feynman diagram such that no colour lines need cross as in the figures above.

E. Born variables and parton flavours for Drell-Yan production

The Born variables Q^2 and Y for each event were distributed according to the Born cross-section in (6.9). Hence the momentum fractions x_q and $x_{\bar{q}}$ given in (6.2) are generated. The flavour of the quarks involved in each event is also determined at the Born level according to the product, $e_{q_i}^2 f_q(x_{q_i}, Q^2) f_{\bar{q}}(x_{\bar{q}_i}, Q^2)$. Colours are assigned in the planar approximation which is correct to $O(\frac{1}{{N_C}^2})$ where $N_C = 3$.

F. Monte Carlo algorithm for Drell-Yan production

The eight integrals listed were evaluated by the 'Hit Or Miss' method and used to generate a set of unweighted events using the importance sampling method described in Section A.

$$
\begin{aligned}
I^{(2)}_{Jq\bar{q}} &= \sum_q \int_J dxdy \left[\frac{x[D_q(x_1,\mu^2)D_{\bar{q}}(x_2,\mu^2)+q\leftrightarrow\bar{q}]}{D_q(x_q)D_{\bar{q}}(x_{\bar{q}})} \frac{1}{2} \left\{ \delta(1-x) + \frac{\alpha_S}{2\pi} C_F \left(\frac{3}{(1-x)_+} \right.\right.\right. \\
&- \left.\left.\left. 6-4x+2(1+x^2)\left(\frac{\ln(1-x)}{1-x} \right)_+ + \left(1+\frac{4}{3}\pi^2 \right)\delta(1-x) \right) \right\} - M_{q\bar{q}} + M_{C_{q\bar{q}}} \right] , \\
I^{(3)}_{Jq\bar{q}} &= \sum_q \int_J dxdy [M_{q\bar{q}} - M_{C_{q\bar{q}}}] , \\
I^{(2)}_{Dq\bar{q}} &= \sum_q \int_J dxdy \left[\frac{x[D_q(x_1,\mu^2)D_{\bar{q}}(x_2,\mu^2)+q\leftrightarrow\bar{q}]}{D_q(x_q)D_{\bar{q}}(x_{\bar{q}})} \frac{1}{2} \left\{ \delta(1-x) + \frac{\alpha_S}{2\pi} C_F \left(\frac{3}{(1-x)_+} \right.\right.\right. \\
&- \left.\left.\left. 6-4x+2(1+x^2)\left(\frac{\ln(1-x)}{1-x} \right)_+ + \left(1+\frac{4}{3}\pi^2 \right)\delta(1-x) \right) \right\} - M_{q\bar{q}} \right] , \\
I^{(3)}_{Dq\bar{q}} &= \sum_q \int_J dxdy M_{q\bar{q}} , \\
I^{(2)}_{Jqg} &= \sum_q \int_J dxdy \left[\frac{x[D_q(x_1,\mu^2)D_g(x_2,\mu^2)+q\leftrightarrow g]}{D_q(x_q)D_{\bar{q}}(x_{\bar{q}})} \frac{\alpha_S}{2\pi} T_F \frac{1}{2} \left\{ \frac{3}{2} - 5x + \frac{9}{2}x^2 \right.\right. \\
&+ \left.\left. (x^2+(1+x^2))\ln(1-x) \right\} - M_{qg} + M_{C_{qg}} \right] , \\
I^{(3)}_{Jqg} &= \sum_q \int_J dxdy [M_{qg} - M_{C_{qg}}] , \\
I^{(2)}_{Dqg} &= \sum_q \int_J dxdy \left[\frac{x[D_q(x_1,\mu^2)D_g(x_2,\mu^2)+q\leftrightarrow g]}{D_q(x_q)D_{\bar{q}}(x_{\bar{q}})} \frac{\alpha_S}{2\pi} T_F \frac{1}{2} \left\{ \frac{3}{2} - 5x + \frac{9}{2}x^2 \right.\right. \\
&+ \left.\left. (x^2+(1+x^2))\ln(1-x) \right\} - M_{qg} \right] , \\
I^{(3)}_{Dqg} &= \sum_q \int_D dxdy M_{qg} . \qquad \text{(F.1)}
\end{aligned}
$$

As in the e^+e^- case, the $I^{(3)}_J$ integrals are negative because $M < M_C$. The integrals are all finite but there are divergences in the integrands which need to be regularized to make the sampling process efficient. This is the subject of Section G. So far we have discussed event generation in the DIS scheme. In the $\overline{\rm MS}$ factorization scheme, the full cross-section ratio is

$$
\begin{aligned}
\frac{\sigma^{NLO}}{\sigma_0} &= \sum_q \int dx_1 dx_2 \left[\frac{x[D_q(x_1,\mu^2)D_{\bar{q}}(x_2,\mu^2)+q\leftrightarrow\bar{q}]}{D_q(x_q)D_{\bar{q}}(x_{\bar{q}})} \left\{ \delta(1-x) + \frac{\alpha_S}{2\pi} C_F \left(-2\frac{1+x^2}{1-x}\ln x \right.\right.\right. \\
&+ \left. 4(1+x^2)\left(\frac{\ln(1-x)}{1-x} \right)_+ + \left(-8+\frac{2}{3}\pi^2 \right)\delta(1-x) \right) \Bigg\} \\
&+ \frac{x[D_q(x_1,\mu^2)D_g(x_2,\mu^2)+q\leftrightarrow g]}{D_q(x_q)D_{\bar{q}}(x_{\bar{q}})} \frac{\alpha_S}{2\pi} T_F \left\{ \frac{1}{2} + 3x - \frac{7}{2}x^2 \right. \\
&+ \left.\left. (x^2+(1+x^2))\ln\frac{(1-x)^2}{x} \right\} \right] . \qquad \text{(F.2)}
\end{aligned}
$$

Hence the corresponding integrals for $\overline{\rm MS}$ scheme event generation are

$$
\begin{aligned}
I^{(2)}_{Jq\bar{q}} &= \sum_q \int_J dxdy \left[\frac{x[D_q(x_1,\mu^2)D_{\bar{q}}(x_2,\mu^2)+q\leftrightarrow\bar{q}]}{D_q(x_q)D_{\bar{q}}(x_{\bar{q}})} \frac{1}{2} \left\{ \delta(1-x) + \frac{\alpha_S}{2\pi} C_F \left(-2\frac{1+x^2}{1-x}\ln x \right.\right.\right. \\
&+ \left.\left.\left. 4(1+x^2)\left(\frac{\ln(1-x)}{1-x}\right)_+ + \left(-8+\frac{2}{3}\pi^2\right)\delta(1-x)\right)\right\} - M_{q\bar{q}} + M_{C_{q\bar{q}}} \right] , \\
I^{(3)}_{Jq\bar{q}} &= \sum_q \int_J dxdy [M_{q\bar{q}} - M_{C_{q\bar{q}}}] , \\
I^{(2)}_{Dq\bar{q}} &= \sum_q \int_J dxdy \left[\frac{x[D_q(x_1,\mu^2)D_{\bar{q}}(x_2,\mu^2)+q\leftrightarrow\bar{q}]}{D_q(x_q)D_{\bar{q}}(x_{\bar{q}})} \frac{1}{2} \left\{ \delta(1-x) + \frac{\alpha_S}{2\pi} C_F \left(-2\frac{1+x^2}{1-x}\ln z \right.\right.\right. \\
&+ \left.\left.\left. 4(1+x^2)\left(\frac{\ln(1-x)}{1-x}\right)_+ + \left(-8+\frac{2}{3}\pi^2\right)\delta(1-x)\right)\right\} - M_{q\bar{q}} \right] , \\
I^{(3)}_{Dq\bar{q}} &= \sum_q \int_J dxdy M_{q\bar{q}} , \\
I^{(2)}_{Jqg} &= \sum_q \int_J dxdy \left[\frac{x[D_q(x_1,\mu^2)D_g(x_2,\mu^2)+q\leftrightarrow g]}{D_q(x_q)D_{\bar{q}}(x_{\bar{q}})} \frac{\alpha_S}{2\pi} T_F \frac{1}{2} \left\{ \frac{1}{2} + 3x - \frac{7}{2}x^2 \right.\right. \\
&+ \left.\left. (x^2+(1+x^2))\ln\frac{(1-x)^2}{x} \right\} - M_{qg} + M_{C_{qg}} \right] , \\
I^{(3)}_{Jqg} &= \sum_q \int_J dxdy [M_{qg} - M_{C_{qg}}] , \\
I^{(2)}_{Dqg} &= \sum_q \int_J dxdy \left[\frac{x[D_q(x_1,\mu^2)D_g(x_2,\mu^2)+q\leftrightarrow g]}{D_q(x_q)D_{\bar{q}}(x_{\bar{q}})} \frac{\alpha_S}{2\pi} T_F \frac{1}{2} \left\{ \frac{1}{2} + 3x - \frac{7}{2}x^2 \right.\right. \\
&+ \left.\left. (x^2+(1+x^2))\ln\frac{(1-x)^2}{x} \right\} - M_{qg} \right] , \\
I^{(3)}_{Dqg} &= \sum_q \int_D dxdy M_{qg} .
\end{aligned}
\tag{F.3}
$$

The divergences and mappings used are discussed in Section G.

G. Divergences and mappings for Drell-Yan production

G.1 Divergences in $M_{q\bar{q}}$ in dead region D

In region D, the hard matrix element:;

$$
M_{q\bar{q}}(x,y) = \frac{D_q(x_1)D_{\bar{q}}(x_2)}{D_q(x_q)D_{\bar{q}}(x_{\bar{q}})} \frac{\alpha_S}{2\pi} C_F \frac{y^2(1-x)^2+(1+x)^2}{(1-x)(1-y^2)} \tag{G.1}
$$

diverges as $(x,y)\to(0,1),(0,-1)$ and $(1,0)$. The mappings used to regularize these divergences are presented.

G.1.1 Region D : $(0,1),(0,-1)$

A simple pole is approached in $M_{q\bar{q}}$ as $(x,y)\to(0,1),(0,-1)$. In the region $x<\frac{1}{4}, y>\frac{3}{5}$, a new set of random points are generated for events which fall between the lines $x=\frac{5}{8}(1-y)$

and $x = 0$. The mapping used and weight factor, w for these points is:

$$\begin{aligned} y^{'} &= 1 - \frac{2}{5} r_1 \,, \\ x^{'} &= \frac{5}{8} r_2 (1 - y^{'}) \,, \\ w &= 2 r_1 \end{aligned} \tag{G.2}$$

where r_1, and r_2 are random numbers in the range $[0:1]$. For the region $x < \frac{1}{4}, y < -\frac{3}{5}$, interchange $y \leftrightarrow -y$. The mapped regions are shown with solid boundaries in Figure 29.

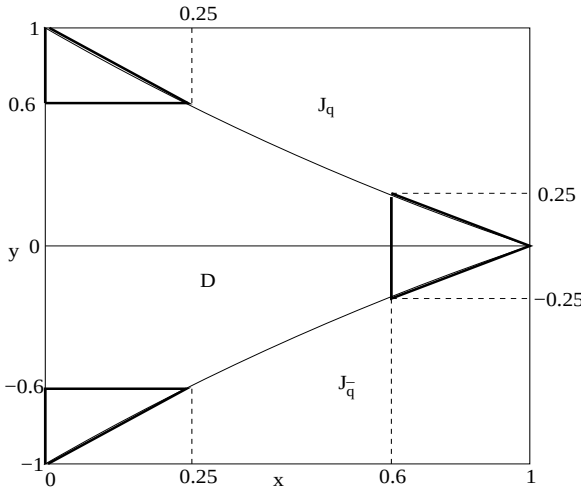

Figure 29: Mapped regions

G.1.2 Region D : $(1, 0)$

As $x \to 1$, there is a pole in $M_{q\bar{q}}$. This divergence is regularized by applying the following mapping and weight factor to points which fall between the lines $y = \frac{5}{8}(1 - x)$ and $y = 0$ within the region $x > \frac{3}{5}, 0 < y < \frac{1}{4}$.

$$\begin{aligned} x^{'} &= 1 - \frac{2}{5} r_1 \,, \\ y^{'} &= \frac{5}{8} r_2 (1 - x^{'}) \,, \\ w &= 2 r_1 \,. \end{aligned} \tag{G.3}$$

In the region $x > \frac{3}{5}, 0 > y > -\frac{1}{4}$, a similar mapping is used;

$$\begin{aligned} x^{'} &= 1 - \frac{2}{5} r_1 \,, \\ y^{'} &= -\frac{5}{8} r_2 (1 - x^{'}) \,, \\ w &= 2 r_1 \,. \end{aligned} \tag{G.4}$$

The mapped regions are shown with solid boundaries in Figure 29.

G.2 Divergences in M_{qg} in dead region D

In region D, the hard matrix element:

$$M_{qg}(x,y) = \frac{D_q(x_1)D_g(x_2)}{D_q(x_q)D_{\bar{q}}(x_{\bar{q}})}\frac{\alpha_S}{2\pi}T_F\frac{(3+y^2)(1-x)^2 - 2y(1-x^2) + 2(1+x^2)}{4(1-y)} \tag{G.5}$$

diverges as $(x,y) \to (0,1)$. for points within the region, $x < \frac{1}{4}, y > \frac{3}{5}$, a new set of random points are generated for events which fall between the lines $x = \frac{5}{8}(1-y)$ and $x = 0$. The mapping used to regularize this divergence is:

$$\begin{aligned} y^{'} &= 1 - \frac{2}{5}r_1\,, \\ x^{'} &= \frac{5}{8}r_2(1-x^{'})\,, \\ w &= 2r_1\,. \end{aligned} \tag{G.6}$$

The mapped region is shown with solid boundaries in Figure 30.

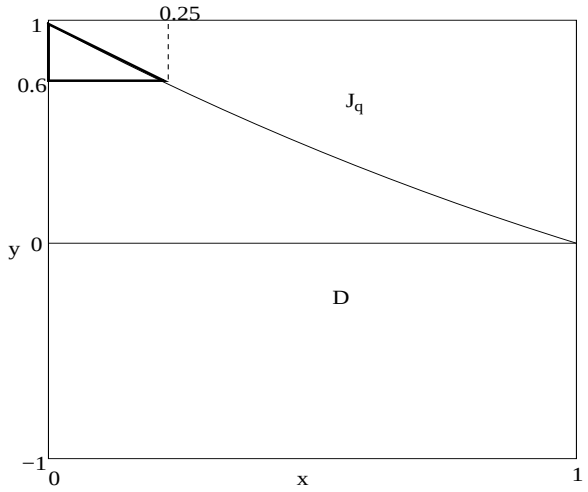

Figure 30: Mapped regions

G.3 Divergences in $(M - M_C)_{q\bar{q}}$ in jet region J

In regions J_q and $J_{\bar{q}}$ depicted in Figure 31, the relevant integral to be evaluated is $M - M_C$ which in region J_q is given by

$$(M - M_C)_{q\bar{q}} = \frac{D_q(x_1)D_{\bar{q}}(x_2)}{D_q(x_q)D_{\bar{q}}(x_{\bar{q}})}\frac{\alpha_S}{2\pi}C_F\frac{(x-1)((x-1)y^2+2y) + (3x+5)(x+1)}{4x(1+y)}\,. \tag{G.7}$$

This diverges as $x \to 0$. There are no singularities at the points $x = 1, y = \pm 1$ because the divergences at these points exactly cancel between M and M_C. Points in the region $x < \frac{1}{8}, y > \frac{3}{4}$ and between the lines $y = 0$ and $y = 1 - 2x$ are mapped and re-weighted

according to (G.8).

$$\begin{aligned} x^{'} &= \frac{1}{8} r_1 \,, \\ y^{'} &= 1 - 2x^{'} r_2 \,, \\ w &= 2r_1 \,. \end{aligned} \tag{G.8}$$

Interchange $y \leftrightarrow -y$ for the region $J_{\bar{q}}$.

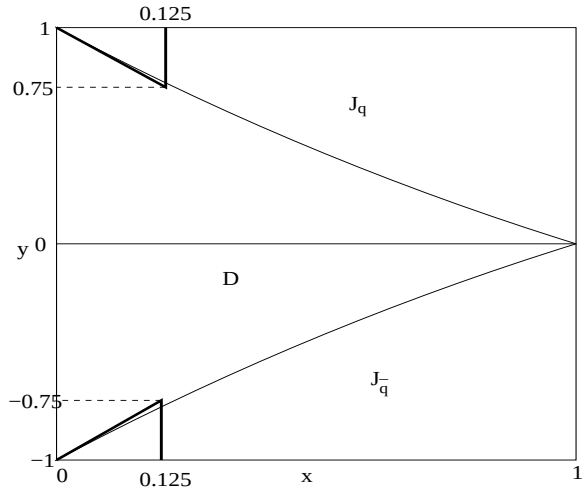

Figure 31: Mapped regions

G.4 Divergences in $(M - M_C)_{qg}$ in jet region J

$(M - M_C)_{qg}$ is given by

$$(M - M_C)_{qg} = \frac{D_q(x_1) D_g(x_2)}{D_q(x_q) D_{\bar{q}}(x_{\bar{q}})} \frac{\alpha_S}{2\pi} T_F \frac{(x-1)[4x^2 - 3x + 1 + 3xy(x-1) + y^2(x-1)^2]}{4x} \tag{G.9}$$

which diverges as $x \to 0$ in region J. This is regularized by using the same mapping presented in (G.8).

References

[1] S. Gieseke *et al.*, "Herwig++ 2.0 release note," `hep-ph/0609306`.

[2] M. H. Seymour, "A simple prescription for first order corrections to quark scattering and annihilation processes," *Nucl. Phys.* **B436** (1995) 443–460, `hep-ph/9410244`.

[3] P. Nason, "A new method for combining NLO QCD with shower Monte Carlo algorithms," *JHEP* **11** (2004) 040, `hep-ph/0409146`.

[4] P. Nason and G. Ridolfi, "A positive-weight next-to-leading-order Monte Carlo for Z pair hadroproduction," *JHEP* **08** (2006) 077, `hep-ph/0606275`.

[5] O. Latunde-Dada, S. Gieseke, and B. Webber, "A positive-weight next-to-leading-order Monte Carlo for e^+e^- annihilation to hadrons," *JHEP* **02** (2007) 051, `hep-ph/0612281`.

[6] S. Frixione, P. Nason, and G. Ridolfi, "A positive-weight next-to-leading-order Monte Carlo for heavy flavour hadroproduction," `arXiv:0707.3088 [hep-ph]`.

[7] S. Frixione, P. Nason, and G. Ridolfi, "The POWHEG-hvq manual version 1.0," `arXiv:0707.3081 [hep-ph]`.

[8] S. Frixione and B. R. Webber, "Matching NLO QCD computations and parton shower simulations," *JHEP* **06** (2002) 029, `hep-ph/0204244`.

[9] S. Frixione and B. R. Webber, "The MC@NLO event generator," `hep-ph/0207182, hep-ph/0612272`.

[10] S. Frixione, P. Nason, and B. R. Webber, "Matching NLO QCD and parton showers in heavy flavour production," *JHEP* **08** (2003) 007, `hep-ph/0305252`.

[11] S. Frixione, E. Laenen, P. Motylinski, and B. R. Webber, "Single-top production in MC@NLO," *JHEP* **03** (2006) 092, `hep-ph/0512250`.

[12] G. Corcella *et al.*, "Herwig 6: An event generator for hadron emission reactions with interfering gluons (including supersymmetric processes)," *JHEP* **01** (2001) 010, `hep-ph/0011363`.

[13] S. Gieseke, A. Ribon, M. H. Seymour, P. Stephens, and B. Webber, "Herwig++ 1.0: An event generator for e^+e^- annihilation," *JHEP* **02** (2004) 005, `hep-ph/0311208`.

[14] R. K. Ellis, W. J. Stirling, and B. R. Webber, "QCD and Collider Physics," *Cambridge University Press* (1996).

[15] S. Gieseke, P. Stephens, and B. Webber, "New formalism for QCD parton showers," *JHEP* **12** (2003) 045, `hep-ph/0310083`.

[16] Y. L. Dokshitzer, V. A. Khoze, and W. J. Stirling, "Gluon radiation and energy losses in top quark production," *Nucl. Phys.* **B428** (1994) 3–18, `hep-ph/9405243`.

[17] A. Djouadi, J. H. Kuhn, and P. M. Zerwas, "B jet asymmetries in Z decays," *Z. Phys.* **C46** (1990) 411–418.

[18] **SLD** Collaboration, K. Abe *et al.*, "Production of pi+, pi-, k+, k-, p and anti-p in light (uds), c and b jets from Z0 decays," *Phys. Rev.* **D69** (2004) 072003, `hep-ex/0310017`.

[19] **DELPHI** Collaboration, P. Abreu *et al.*, "Tuning and test of fragmentation models based on identified particles and precision event shape data," *Z. Phys.* **C73** (1996) 11–60.

[20] G. Altarelli, R. K. Ellis, and G. Martinelli, "Leptoproduction and Drell-Yan processes beyond the leading approximation in chromodynamics," *Nucl. Phys.* **B143** (1978) 521.

[21] L. N. Lipatov, "The parton model and perturbation theory," *Sov. J. Nucl. Phys.* **20** (1975) 94–102.

[22] V. N. Gribov and L. N. Lipatov, "e^+e^- pair annihilation and deep inelastic e p scattering in perturbation theory," *Sov. J. Nucl. Phys.* **15** (1972) 675–684.

[23] G. Altarelli and G. Parisi, "Asymptotic freedom in parton language," *Nucl. Phys.* **B126** (1977) 298.

[24] Y. L. Dokshitzer, "Calculation of the structure functions for deep inelastic scattering and e^+e^- annihilation by perturbation theory in Quantum Chromodynamics. (in russian)," *Sov. Phys. JETP* **46** (1977) 641–653.

[25] A. S. Ito *et al.*, "Measurement of the continuum of dimuons produced in high- energy proton - nucleus collisions," *Phys. Rev.* **D23** (1981) 604.

[26] **CDF** Collaboration, A. A. Affolder *et al.*, "The transverse momentum and total cross section of e^+e^- pairs in the Z boson region from $p\bar{p}$ collisions at $\sqrt{s} = 1.8$ TeV," *Phys. Rev. Lett.* **84** (2000) 845–850, `hep-ex/0001021`.

[27] **D0** Collaboration, V. M. Abazov *et al.*, "Measurement of the shape of the boson rapidity distribution for $p\bar{p} \to$ Z / $\gamma^* \to e^+e^-$+ X events produced at $\sqrt{s}$ of 1.96 TeV," *Phys. Rev.* **D76** (2007) 012003, `hep-ex/0702025`.

[28] G. P. Lepage, "VEGAS: An adaptive multidimensional integration program,". CLNS-80/447.

[29] R. Kleiss, "From two to three jets in heavy boson decays: An algorithmic approach," *Phys. Lett.* **B180** (1986) 400.